JAERI-M
9752

STUDY ON MODELING OF PIPE WHIPPING BY FINITE ELEMENT METHOD

October 1981

Noriyuki MIYAZAKI, Shuzo UEDA, Ryoichi KURIHARA,
Kazuo SAITO,* Rokuro KATO and Toshikuni ISOZAKI

日本原子力研究所
Japan Atomic Energy Research Institute

この報告書は，日本原子力研究所がJAERI-Mレポートとして，不定期に刊行している研究報告書です．入手，複製などのお問合わせは，日本原子力研究所技術情報部（茨城県那珂郡東海村）あて，お申しこしください．

JAERI-M reports, issued irregularly, describe the results of research works carried out in JAERI. Inquiries about the availability of reports and their reproduction should be addressed to Division of Technical Information, Japan Atomic Energy Research Institute, Tokai-mura, Naka-gun, Ibaraki-ken, Japan.

JAERI-M 9752

Study on Modeling of Pipe Whipping by Finite Element Method

Noriyuki MIYAZAKI, Shuzo UEDA, Ryoichi KURIHARA
Kazuo SAITO*, Rokuro KATO and Toshikuni ISOZAKI

Division of Reactor Safety, Tokai Research Establishment, JAERI

(Received September 24, 1981)

The general purpose finite element codes ADINA and MARC were used to make a preliminary analysis for the pipe whip tests performed with use of 4B, sch80 test pipes under the saturated water condition (pressure = 69 kg/cm^{2}G, temperature = 284.5 °C). In the analysis the initial clearance between the test pipe and the restraints was taken to be equal to 30 mm, 50 mm and 100 mm for RUN No. 5405, 5406 and 5407, respectively. On the other hand, the overhang length was kept equal to 400 mm for the above three cases. The experimental result of the jet discharge test, RUN No. 5401, and the analytical results obtained from the PRTHRUST-J1 code for calculation of blowdown thrust force were used as the time history of loading of the pipe whip analyses. In the analyses, various models of the test pipe and the restraints were employed to study the effect of modeling on the pipe whip behavior and the guides to the analysis of pipe whip in the future are also presented.

Keywords; Finite Element Codes, Pipe Whip Tests, Restraint, Clearance, Overhang Length, Blowdown Thrust Force , BWR

This work was performed under the contract between the Science and Technology Agency of Japan and JAERI to demonstrate the safety for pipe rupture of the primary coolant circuits in nuclear power plants.

* On leave from Ishikawajima Harima Heavy Industries Co., Ltd.

有限要素法によるパイプホイップ解析のモデル化について

日本原子力研究所東海研究所安全工学部
宮崎　則幸・植田　脩三・栗原　良一
斉藤　和男*・加藤　六郎・磯崎　敏邦

（1981年9月24日受理）

4B, sch 80試験配管によるBWR，飽和水条件下（系内圧力＝69 kg/cm²G，系内温度＝284.5℃）でのパイプホイップ試験について，汎用有限要素法解析コード，ADINAおよびMARCを用いて予備解析を実施した。解析は実際行われる試験を考慮して，オーバハングを400 mm一定とし，配管とレストレントとの間の初期クリアランスが30 mm（RUN No. 5405），50 mm（RUN No. 5406）および100 mm（RUN No. 5407）の各場合について実施した。また配管に加わるブローダウンスラスト力としては曲管ジェット試験（RUN No. 5401）の試験結果，およびブローダウンスラスト力解析コードPRTHRUST－J1による解析結果を用いた。配管およびレストレントのモデル化の方法について種々の検討を行い，今後の解析の指針を与えた。

この報告書は，電源開発促進対策特別会計施行令に基づき，科学技術庁から日本原子力研究所への委託研究，昭和54年度配管信頼性実証試験のうちでADINAおよびMARCコードによるパイプホイップ解析のモデル化の検討結果をまとめたものである。

＊　外来研究員：石川島播磨重工業（株）

CONTENTS

目　　次

1. INTRODUCTION

Three cases of pipe whip tests, RUN No. 5405, 5406 and 5407, were performed under the saturated water condition (pressure = 69 kg/cm^{2}G, temperature = 284.5 °C) with use of 4B, sch80 test pipes. In the tests, overhang length was taken to be equal to 400 mm. On the other hand, the initial clearance between the test pipe and the restraints was taken to be equal to 30 mm, 50 mm and 100 mm for RUN No. 5405, 5406 and 5407, respectively, to study the effects of initial clearance on the pipe whip behavior.

This report presents the results of preliminary analysis which was carried out by the general purpose finite element codes ADINA and MARC. The experimental result of the jet dicharge test, RUN No. 5401[2], and the analytical results obtained from the PRTHRUST-J1 code[3](*1) were used as the time history of loading. Various models were considered for the test pipe and the restraints in the analyses by the ADINA code. Analyses were also performed by taking account of the effect of geometrical nonlinearity of the test pipe. In the analyses by the MARC code, shell elements were used in the elbow. The effects of finite element modeling of the test pipe and the restraints on the pipe whip behavior were studied by assessing the results obtained from the analyses of various models.

In this report, Chapter 2 describes the outline of pipe whip tests, RUN No. 5405, 5406 and 5407. Chapter 3 describes the various analytical models, the time histories of loading and the material constants used in the analyses by the ADINA and MARC codes. Analytical results are shown in Chapter 4. Furthermore, the main conclusions and guides of the analysis in the future are given in Chapter 5.

2. PIPE WHIP TESTS, RUN NO. 5405, 5406 AND 5407

The pipe whip tests, RUN No. 5405, 5406 and 5407, were performed under the saturated water condition (pressure = 69 kg/cm^{2}G, temperature = 284.5 °C) with use of 4B, sch80 test pipes. In the tests, the overhang length was taken to be equal to 400 mm. The initial clearance was taken to be equal to 30 mm (RUN No. 5405), 50 mm (RUN No. 5406) and 100

(*1) This code is based on PRTHRUST code developed by Quadrex Corporation.

1. INTRODUCTION

Three cases of pipe whip tests, RUN No. 5405, 5406 and 5407, were performed under the saturated water condition (pressure = 69 kg/cm^{2}G, temperature = 284.5 °C) with use of 4B, sch80 test pipes. In the tests, overhang length was taken to be equal to 400 mm. On the other hand, the initial clearance between the test pipe and the restraints was taken to be equal to 30 mm, 50 mm and 100 mm for RUN No. 5405, 5406 and 5407, respectively, to study the effects of initial clearance on the pipe whip behavior.

This report presents the results of preliminary analysis which was carried out by the general purpose finite element codes ADINA and MARC. The experimental result of the jet dicharge test, RUN No. 5401[2], and the analytical results obtained from the PRTHRUST-J1 code [3](*1) were used as the time history of loading. Various models were considered for the test pipe and the restraints in the analyses by the ADINA code. Analyses were also performed by taking account of the effect of geometrical nonlinearity of the test pipe. In the analyses by the MARC code, shell elements were used in the elbow. The effects of finite element modeling of the test pipe and the restraints on the pipe whip behavior were studied by assessing the results obtained from the analyses of various models.

In this report, Chapter 2 describes the outline of pipe whip tests, RUN No. 5405, 5406 and 5407. Chapter 3 describes the various analytical models, the time histories of loading and the material constants used in the analyses by the ADINA and MARC codes. Analytical results are shown in Chapter 4. Furthermore, the main conclusions and guides of the analysis in the future are given in Chapter 5.

2. PIPE WHIP TESTS, RUN NO. 5405, 5406 AND 5407

The pipe whip tests, RUN No. 5405, 5406 and 5407, were performed under the saturated water condition (pressure = 69 kg/cm^{2}G, temperature = 284.5 °C) with use of 4B, sch80 test pipes. In the tests, the overhang length was taken to be equal to 400 mm. The initial clearance was taken to be equal to 30 mm (RUN No. 5405), 50 mm (RUN No. 5406) and 100

(*1) This code is based on PRTHRUST code developed by Quadrex Corporation.

mm (RUN No. 5407). Saturated water was discharged by breaking the rupture disk attached to the end of the test pipe. Then, the pipe whipping was caused by the blowdown thrust force acting on the test pipe. The dynamic behavior of the test pipe and the restraints were measured by strain gages.

Fig. 1 shows the dimensions of the test pipe made of SUS304 stainless steel. The test pipe was supported by the pipe support at which the test pipe behaved as a fixed end. Therefore, analytical region was taken between the fixed end and the loaded end.

As shown in Fig. 1, four restraints were installed at the position where the overhang length was 400 mm. Fig. 2 shows the dimensions of the restraint. Three kinds of restraints were used for the initial clearance of 30 mm, 50 mm and 100 mm, respectively. These restraints were also made of SUS304 stainless steel.

3. ANALYTICAL MODEL

3.1 Material Constants Used in the Analyses

For the pipe material, the following data were used in the analyses;

E (Young's modulus) = 18,000 kg/mm^2

ν (Poisson ratio) = 0.28

σ_y(Yield stress) = 16 kg/mm^2

E_T(Strain hardening modulus) =256.3 kg/mm^2

These are corresponding to the data of SUS304 stainless steel at the temperature of 300 °C presented in Ref.(4).

On the other hand, the multi-linear approximated stress-strain curve shown in Fig. 3 was used for the restraint material.

3.2 Blowdown Thrust Force Used in the Analyses

In the present analyses, the followings were used for the time history of blowdown thrust force caused by instantaneous pipe break. One was the experimental result of the jet discharge test, RUN No. 5407[(2)]. This is shown in Fig. 4 where the experimental result was approximated by the solid line to be used in the pipe whip analyses.

mm (RUN No. 5407). Saturated water was discharged by breaking the rupture disk attached to the end of the test pipe. Then, the pipe whipping was caused by the blowdown thrust force acting on the test pipe. The dynamic behavior of the test pipe and the restraints were measured by strain gages.

Fig. 1 shows the dimensions of the test pipe made of SUS304 stainless steel. The test pipe was supported by the pipe support at which the test pipe behaved as a fixed end. Therefore, analytical region was taken between the fixed end and the loaded end.

As shown in Fig. 1, four restraints were installed at the position where the overhang length was 400 mm. Fig. 2 shows the dimensions of the restraint. Three kinds of restraints were used for the initial clearance of 30 mm, 50 mm and 100 mm, respectively. These restraints were also made of SUS304 stainless steel.

3. ANALYTICAL MODEL

3.1 Material Constants Used in the Analyses

For the pipe material, the following data were used in the analyses;

E (Young's modulus) = 18,000 kg/mm^2

ν (Poisson ratio) = 0.28

σ_y(Yield stress) = 16 kg/mm^2

E_T(Strain hardening modulus) =256.3 kg/mm^2

These are corresponding to the data of SUS304 stainless steel at the temperature of 300 °C presented in Ref.(4).

On the other hand, the multi-linear approximated stress-strain curve shown in Fig. 3 was used for the restraint material.

3.2 Blowdown Thrust Force Used in the Analyses

In the present analyses, the followings were used for the time history of blowdown thrust force caused by instantaneous pipe break. One was the experimental result of the jet discharge test, RUN No. 5407[(2)]. This is shown in Fig. 4 where the experimental result was approximated by the solid line to be used in the pipe whip analyses.

The other was the analytical results obtained from the PRTHRUST-J1 code for calculation of blowdown thrust force. As shown in Fig. 5, blowdown thrust forces were calculated for the discharge coefficient C_D of 1.0, 0.8 and 0.6. Then, these results were also approximated by the solid lines to be used in the pipe whip analyses.

3.3 Analytical Model for the ADINA Code

In the pipe whip analyses by the ADINA code, the following three analytical models were considered.

(1) Model 1 --- Mass Model

Fig. 6(a) shows the Model 1 of Mass Model. The test pipe was modeled as an assemblage of straight beam elements with annular cross section. A concentrated mass was added to the loaded point of the beam element to represent the mass of the elbow and the short pipe welded to this elbow, while consistent mass was used to represent the remainder of the test pipe. Four restraints were represented by one truss element. In this model, the numbers of nodes, straight beam elements and truss element were 12, 10 and 1, respectively.

(2) Model 2 --- Multi Truss Model

Fig. 6(b) shows the Model 2 of Multi Truss Model. The modeling of the test pipe was same as Model 1, while four restraints were modeled by four truss elements. In this model, the numbers of nodes, straight beam elements and truss elements were 18, 13 and 4, respectively.

(3) Model 3 --- Bend Model

Fig. 6(c) shows the Model 3 of Bend Model. In this model, fifteen straight beam elements were used to model the elbow instead of adding concentrated mass to the loaded point of the test pipe. On the other hand, four restraints were represented by one truss element. In this model, the numbers of nodes, straight beam elements and truss element were 17, 15 and 1, respectively. For this model, comparison was made between the results with and without consideration of the effect of geometrical nonlinearity of the test pipe.(*2)

The cross-sectional areas were 402.12 mm^2 for Models 1 and 3, and

---

(*2) The second order term in the strain-displacement relation is considered in the analyses with geometrical nonlinearity.

100.53 mm^2 for Model 2. According to Fig. 2, truss elements were 435 mm, 466.5 mm and 545 mm long for the initial clearance of 30 mm, 50 mm and 100 mm, respectively. In the analyses, effective clearance was used instead of intial clearance. The meaning and the calculation procedure of the effective clearance are given in Ref.(6). The effective clearance (C_E) were 46.11 mm, 75.92 mm and 148.05 mm for the initial clearance of 30 mm, 50 mm and 100 mm, respectively.

3.4 Analytical Model for the MARC Code

It is well known that the elbow subjected to bending load gives larger deflection than that predicted by the curved beam theory due to decrease of stiffness caused by ovaling of cross section. Then, in the analyses by the MARC code, shell elements were used in the elbow region to study the effects of the shell behavior of the elbow on the pipe whipping.

In the MARC code, the element named Element 17[7] can be used to represent the shell behavior of the elbow. This element is formed by combining the displacement mode of axisymmetric torus with that of beam. In this element, the displacement in the cross section is assumed to be Hermite third order polynomial, whereas the displacement along the longitudinal axis of torus is assumed to be constant.

Fig. 7 shows the finite element breakdown in the analyses by the MARC code. Straight beam elements with pipe cross section (Element 14) were used in the straight pipe region, while the abovementioned shell elements (Element 17) were used in the elbow region. On the other hand, truss element (Element 9) and gap element (Element 12) were used to represent the restraints and the clearance between the test pipe and the restraints, respectively. In the analyses by the MARC code, the numbers of Element 14, Element 17, Element 9 and Element 12 were 11, 24, 1 and 1, respectively. The total numbers of nodes and degrees-of-freedom were 59 and 159, respectively.

The cross-sectional area of truss element was 402.12 mm^2, because four restraints were represented by one truss element. Truss elements were 435 mm, 466.5 mm and 545 mm long for the initial clearance of 30 mm, 50 mm and 100 mm, respectively. Consistent mass was used in the straight pipe region, while a concentrated mass was used in the elbow region. The same data described in Section 3.1 and the experimental result of

the jet discharge test, RUN No. 5401, were used as the material properties and the time history of blowdown thrust force, respectively. Geometrical nonlinearity is not considered in the analyses by the MARC code.

4. ANALYTICAL RESULTS AND DISCUSSION

4.1 Analytical Results by the ADINA Code

4.1.1 Comparisons among Various Models

Analysis was carried out for RUN No. 5405 by the Model 1 of Mass Model, the Model 2 of Multi Truss Model and the Model 3 of Bend Model to study the effects of modeling of the test pipe and the restraints on the pipe whip behavior. The time history of loading obtained from the jet discharge test, RUN No. 5401, was used in the analysis. Geometrical nonlinearity of the test pipe was also taken into account for the analyses using Model 3.

In Fig. 8.1 to Fig. 8.5, comparisons among three models are shown for the time histories of pipe deflection at the loaded point, pipe deflection at the restraint, fiber strain of the pipe at the restraint, restraint strain and the distribution of pipe deflection at the time when the restraint displacement reaches maximum. The signatures R1, R2, R3 and R4 in Figs. 8.2 and 8.4 denote the indices of the restraint numbered sequentialy from rupture disk side. It is found from Figs. 8.1 and 8.5 that there is little difference among three models in the time history of pipe deflection at the time when restraint displacement reaches maximum. It is found from Fig. 8.2 that little difference can be seen between Bend Model and Mass Model in the pipe deflection at the restraint and that the results of these two models are almost coincident with the average of the results of Multi Truss Model. Next, comparing the results of fiber strain of the pipe obtained from these models, as shown in Fig. 8.3, there is a difference of 10 % in the peak values. In other respects, there is no essential difference among three models. Furthermore, the behavior of restraint strain is discussed. As shown in Fig. 8.4, significant difference cannot be observed both results of Bend Model and Mass Model in which one truss element was used to represent four restraint, while in the Multi Truss Model where four

the jet discharge test, RUN No. 5401, were used as the material properties and the time history of blowdown thrust force, respectively. Geometrical nonlinearity is not considered in the analyses by the MARC code.

4. ANALYTICAL RESULTS AND DISCUSSION

4.1 Analytical Results by the ADINA Code

4.1.1 Comparisons among Various Models

Analysis was carried out for RUN No. 5405 by the Model 1 of Mass Model, the Model 2 of Multi Truss Model and the Model 3 of Bend Model to study the effects of modeling of the test pipe and the restraints on the pipe whip behavior. The time history of loading obtained from the jet discharge test, RUN No. 5401, was used in the analysis. Geometrical nonlinearity of the test pipe was also taken into account for the analyses using Model 3.

In Fig. 8.1 to Fig. 8.5, comparisons among three models are shown for the time histories of pipe deflection at the loaded point, pipe deflection at the restraint, fiber strain of the pipe at the restraint, restraint strain and the distribution of pipe deflection at the time when the restraint displacement reaches maximum. The signatures R1, R2, R3 and R4 in Figs. 8.2 and 8.4 denote the indices of the restraint numbered sequentialy from rupture disk side. It is found from Figs. 8.1 and 8.5 that there is little difference among three models in the time history of pipe deflection at the time when restraint displacement reaches maximum. It is found from Fig. 8.2 that little difference can be seen between Bend Model and Mass Model in the pipe deflection at the restraint and that the results of these two models are almost coincident with the average of the results of Multi Truss Model. Next, comparing the results of fiber strain of the pipe obtained from these models, as shown in Fig. 8.3, there is a difference of 10 % in the peak values. In other respects, there is no essential difference among three models. Furthermore, the behavior of restraint strain is discussed. As shown in Fig. 8.4, significant difference cannot be observed both results of Bend Model and Mass Model in which one truss element was used to represent four restraint, while in the Multi Truss Model where four

truss element was used to model four restraints the maximum strain arises in the restraint R1 and maximum strain decreases in sequence of the restraints, R2, R3 and R4. The average strain of four truss elements in Multi Truss Model is, however, almost conincident with the results of other two models. This indicates that it is allowable to model pulral restraints with one truss element when primary concern is average behavior of restraint such as ability of energy absorption and reaction force to a restraint support. Furthermore, Mass Model and Bend Model are preferable to Multi Truss Model in view of numerical stability. Namely, for Multi Truss Model, extreamly high stress arises sometimes in the beam element, at the both ends of which truss elements are allocated.

Fig. 9.1 to Fig. 9.5 show the same results as presented in Fig. 8.1 to Fig. 8.5 between the analyses with and without geometrical nonlinearity. Significant difference connot be seen between these two kinds of analyses. This may be due to the following reason. One end of the test pipe is free, so that large resultant force does not appear in the test pipe even when it undegoes large rotation. Then, the effect of geometrical nonlinearity is not important to the present pipe whip analyses.

4.1.2 Analytical Results of RUN No. 5405, 5406 and 5407

Analytical results are presented here for each pipe whip test. In the analysis, the Model 3 of Bend Model was used and the effect of geometrical nonlinearity was taken into account. Four kinds of time histories of loading were used, viz. the experimental result of the jet discharge test, RUN No. 5401, and the analytical results obtained from the PRTHRUST-J1 code, in which the discharge coefficient C_D were taken to be equal to 1.0, 0.8 and 0.6.

In Fig. 10.1 to Fig. 10.3, Fig. 11.1 to Fig. 11.3, Fig. 12.1 to Fig. 12.3 and Fig. 13.1 to Fig. 13.3 are shown the time histories of pipe deflection at the loaded point, pipe deflection at the restraint, fiber strain of the pipe at the restraint and restraint strain, respectively. It is observed from the figures that the analyses using the results of the PRTHRUST-J1 code give the higher peak values and earlier times in the rising of the curves than those using the experimental result of the jet discharge test, RUN No. 5401. This is due to the reason that, as shown in Figs. 4 and 5, the loadings obtained from PRTHRUST-J1 code is larger than that of the experimental result especially

within time of 15 msec. Table 1 shows the comparison of maximum restraint reaction force among various loadings. Compared with restraint strain, restraint reaction force is less dependent on the loadings used in the analyses. This is because stress becomes less sensitive to strain, since as shown in Fig. 3 the slope of the stress-strain curve decreases in the plastic range.

4.2 Analytical Results by the MARC Code

Analytical results by the MARC code are shown in this section. In the analyses, the elbow part was modeled by shell elements. Fig. 14.1 to Fig. 14.3 show the time histories of pipe deflection at the restraint for the initial clearance of 30 mm, 50 mm and 100 mm. Fig. 15 shows the time history of restraint strain. In these figures, the results obtained from the ADINA code are also depicted with the broken lines. From Fig. 14.1 through Fig. 14.3, fairly good agreement is found between the results of pipe deflection at the restraint by the ADINA and MARC codes before the test pipe impinges on the restraints. On the other hand, the MARC code provides smaller peak deflection of the pipe at the restraint, smaller strain of the restraint and the shorter time required for reaching peak value than the ADINA code. The difference in the results between two codes is thought to be due to the reason that there is a difference in the modeling of the elbow part between these codes. Namely, in the analyses by the MARC code, shell elements were used to model the elbow part, while straight beam elements were used in the analyses by the ADINA code. Therefore, the deformation of the cross section in the elbow was not taken into account in the analyses by the ADINA code. Fig. 16.1 to Fig. 16.3 show the deformation of the cross section in the elbow for the initial clearance of 30 mm, 50 mm and 100 mm. The MARC code may provide smaller deflection of the pipe at the restraint than the ADINA code since a part of kinetic energy of pipe is absorbed as the strain energy due to the deformation of the cross section in the elbow. However, equivalent stress in the elbow is less than 10 kg/mm^2, so that the deformation in the elbow is within elastic range. Then, the strain energy due to the deformation of the cross section in the elbow is so small that the difference in the restraint strain between two codes cannot be explained by this reason. Therefore, the disagreement of the analytical results between two codes may be due to the difference in

such solution algorithms regarding to nonlinear problem as a correction of unbalanced force within a time increment.

Table 2 shows the comparison of maximum reaction force of the restraint between the ADINA and MARC codes. The difference of this quantity is smaller than that of the restraint strain shown in Fig. 15 due to the same reason as described in Section 4.1.

In the analysis, the deformation of cross section in the elbow is not important to the pipe whip behavior, because the moment acting on the first elbow is very small due to the short moment arm. Fig. 17 shows the example where the shell behavior of the second elbow should be taken into consideration in the analysis. In this case, large moment acts on the second elbow, so that it is reasonable to use shell elements to model the second elbow.

4.3 Some Considerations on Analytical Limitations of the ADINA and MARC Codes

As described in Ref. (5) and (6), in the analysis by the ADINA code, the clearance between the test pipe and the restraint is included in OA of the stress-strain curve of the nonlinear elastic truss element. In this analysis, the unloading path from maximum point C is the reverse of loading path, viz. C→B→A→O in Fig. 18(a). Therefore, the analytical results of the ADINA code are supposed to be unreliable after the restraint displacement reaches maximum because the unloading from plastic state to elastic state cannot be treated by the modeling technique used in the analyses by the ADINA code.

On the other hand, in the analyses by the MARC code, the clearance and restraint are modeled by gap element and truss element, respectively. Therefore, it is not necessary in the analyses by the MARC code to include the effect of clearance in the stress-strain curve of truss element. Then, the isotropic strain hardening plastic model was used for truss element. In this case, the unloading path descends from B to D shown in Fig. 18(b), because the gap element used in the analyses cannot represent the increase of clearance (δ in Fig. 18(b)) due to plastic deformation. Strictly speaking, the test pipe must be detached from the restraints at point C in the unloading process. According to the above reason, the MARC code provides reliable result so far as point C in Fig. 18(b).

5. CONCLUDING REMARKS

This paper presents the results of the preliminary analysis for the pipe whip tests, RUN No. 5405, 5406 and 5407 and the comparison of the results obtained from various models with use of the general purpose finite element codes, ADINA and MARC.

The following conclusions are obtained from the analyses by the ADINA code.

(1) Comparing the results of Multi Truss Model in which four truss elements were used to model four restraints with those of Mass Model or Bend Model where four restraints were represented by one truss element, significant difference cannot be observed in such average behaviors of the restraints as average strain of restraints, total reaction force of restraint and ability of energy absorption of restraints. It is also found that in view of numerical stability the latter models are preferable to the former one.

(2) Regarding to modeling of the elbow, there is little difference between Mass Model in which the elbow is modeled as a concentrated mass and Bend Model where the elbow is represented by several straight beam elements.

(3) Geometrical nonlinearity is not important to the problem presented here.

(4) The analyses using the load-time functions obtained from the PRTHRUST-J1 code give safer results than those using the load-time function obtained from the jet discharge test, RUN No. 5401.

Furthermore, the following conclusions are obtained from the analyses by the MARC code.

(5) The deformation in the cross section in the first elbow adjacent to the break point is within elastic range, so that the energy absorption by this deformation is very small.

(6) Compared with the results by the ADINA code, the MARC code does not predict safe results for the pipe whip problem.

In addition to the above conclusions,

(7) The analytical limitations of the ADINA and MARC codes are made clear.

Finally, the guidline for future analysis are presented as follows

(1) It is recommended that one truss element with same cross-sectional area as total one of pulral restraints is used to model the restraints,

when primary concern is average behavior of the restraint such as average strain of restraints, ability of energy absorption of restraint and reaction force to restraint support. On the other hand, plural restraints should be modeled by the same number of truss elements, when the strain and reaction force of each restraint are required. However, it is noted that numerical instability occurs sometimes in the latter case.

(2) It is recommended that the part of the test pipe from the first elbow to the break point is modeled by attaching a concentrated mass corresponding to this part to the straight beam elements. On the other hand, shell element should be used for the second elbow shown in Fig. 17.

ACKNOWLEDGEMENTS

The authors wish to make their grateful acknowledgement to Dr. S. Miyazono, Chief of the Mechnical Strength and Structure Laboratory in JAERI.

when primary concern is average behavior of the restraint such as average strain of restraints, ability of energy absorption of restraint and reaction force to restraint support. On the other hand, plural restraints should be modeled by the same number of truss elements, when the strain and reaction force of each restraint are required. However, it is noted that numerical instability occurs sometimes in the latter case.

(2) It is recommended that the part of the test pipe from the first elbow to the break point is modeled by attaching a concentrated mass corresponding to this part to the straight beam elements. On the other hand, shell element should be used for the second elbow shown in Fig. 17.

ACKNOWLEDGEMENTS

The authors wish to make their grateful acknowledgement to Dr. S. Miyazono, Chief of the Mechnical Strength and Structure Laboratory in JAERI.

REFERENCES

(1) Isozaki, T., Ueda, S., Kannoto, Y., Kurihara, R., Matsumoto, M., Miyazaki, N., Hashimoto, M. and Miyazono, S., "Outline of Facilities for Pipe Rupture Test", 1978 Fall Meeting Reactor Phys. & Eng., At. Energy Soc. Japan, (in Japanese), C4 (1978).

(2) Isozaki, T., Ueda, S., Miyazaki, N., Kato, R., Kurihara, R., Saito, K. and Miyazono, S., "Test Results of Discharging Jet from 4B Pipes (RUN No. = 5401, 5402, 5403, 5404)", Unpublished Report, (in Japanese).

(3) Miyazaki, N. and Kogo, J., "Outline of PRTHRUST Code and PRTHRUST-J1 Code for Calculating Blowdown Thrust Force", JAERI-M 9137 (1980).

(4) "Study on Practical Use of Nonlinear Structural Analysis (I)", Japan Soc. Mech. Eng., (in Japanese) (1977), Fig. 14 in pp.116.

(5) Miyazaki, N., Kannoto, Y., and Kurihara, R., "A Parametric Analysis of Pipe Whip Behavior (4B, sch-80 Pipe, BWR Condition)", J. At. Energy Soc. Japan, (in Japanese), Vol.21, No.6 (1979), pp.518-529.

(6) Miyazaki, N. and Saito, K., "Preliminaly Analysis for Pipe Whip Test - RUN No. 5319", JAERI-M 8487 (1979).

(7) Marcal, P.V., "Elastic-Plastic Behaviour of Pipe Bend with In-Plane Bending", J. Strain Analysis, Vol.2, No.1 (1967), pp.84-90.

Captions of Tables and Figures

Table 1 Comparison of maximum restraint reaction force among various loading

F(t)		Maximum Restraint Reaction Force (kgf)		
		CL = 30	CL = 50	CL = 100
RUN No. 5401		15632	16363	17834
PRTHRUST-J1	$C_D = 1.0$	17251	18145	19444
	$C_D = 0.8$	16916	17646	19222
	$C_D = 0.6$	16448	17237	18966

F(t) = Time history of blowdown thrust force used in the pipe whip analyses.

C_D = Discharge coefficient

CL = Initial clearance (mm)

Table 2 Comparison of maximum restraint reaction force between the MARC and ADINA codes

Code Name	Maximum Restraint Reaction Force (kgf)		
	CL = 30	CL = 50	CL = 100
MARC	14663	15711	16331
ADINA	15632	16363	17834

CL = Initial clearance

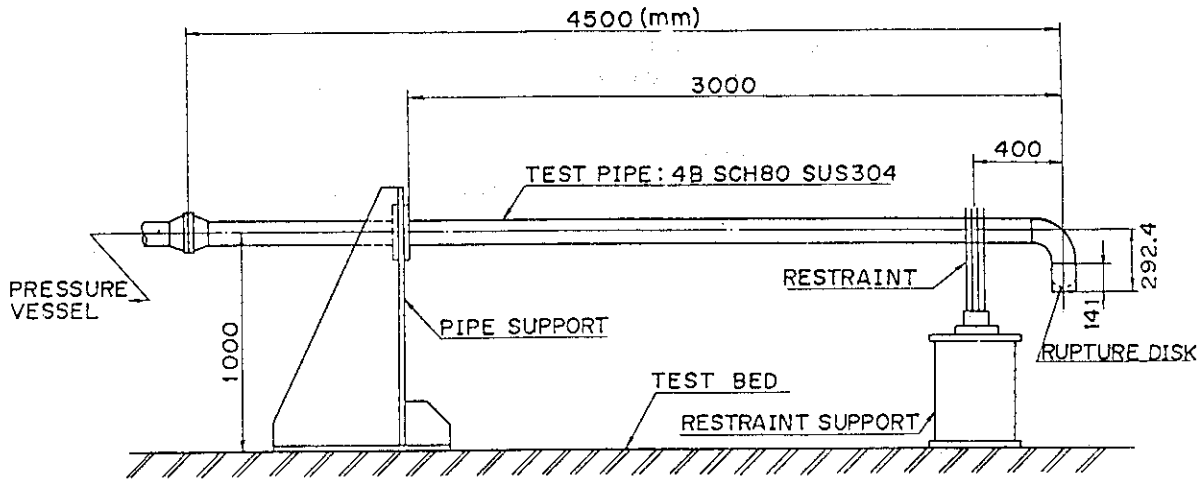

Fig. 1 Dimensions of test pipe

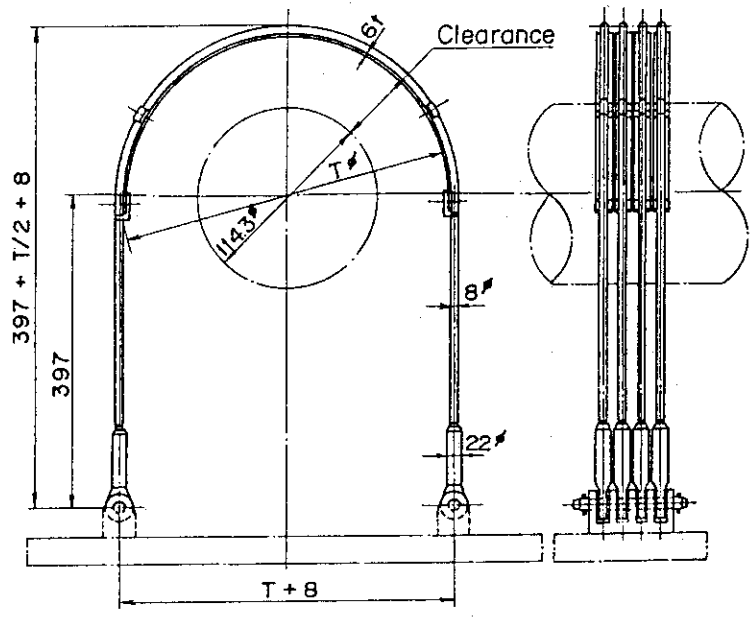

	RUN NO.	Clearance (mm)	T (mm)
①	5405	30	186.3
②	5406	50	226.3
③	5407	100	326.3

Fig. 2 Dimensions of restraints

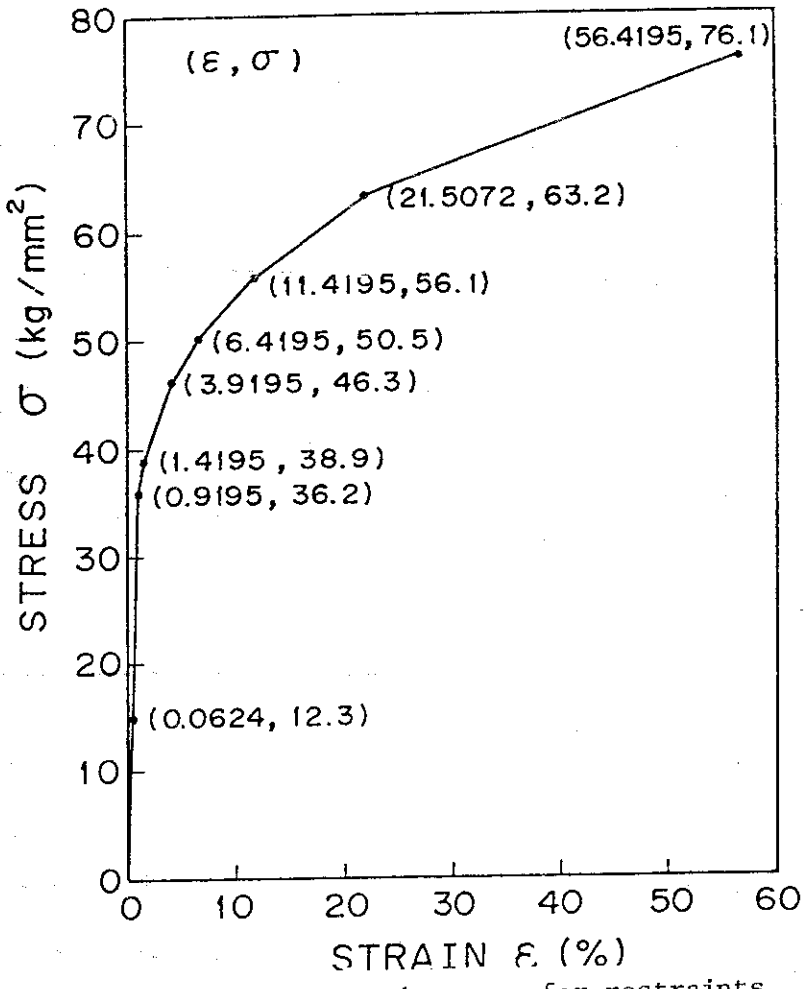

Fig. 3 Stress-strain curve for restraints

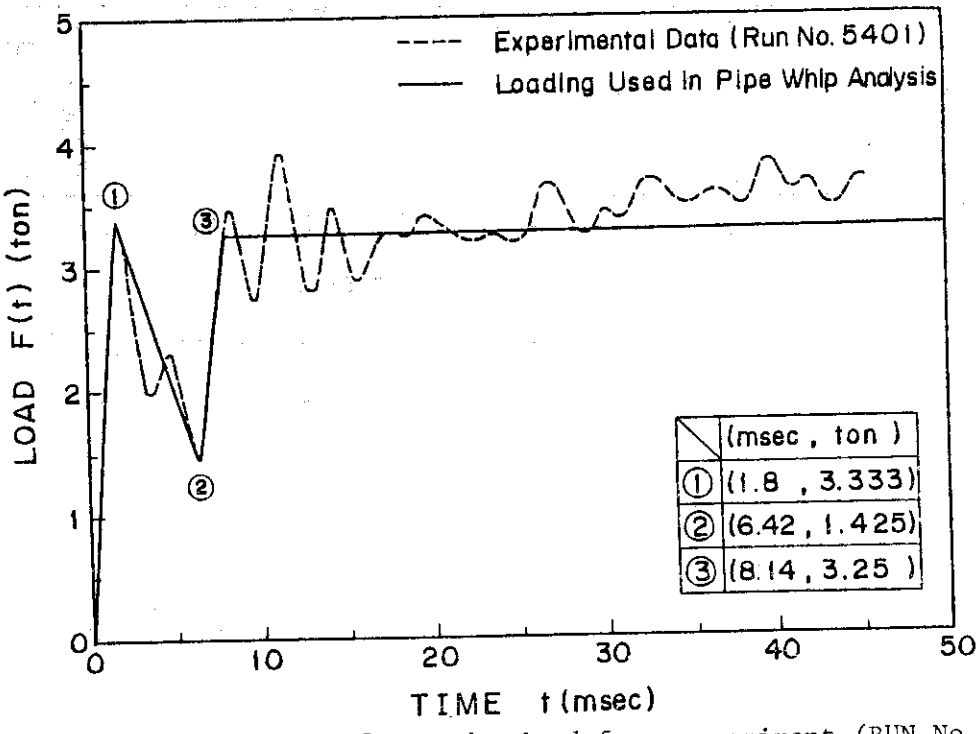

Fig. 4 Blowdown thrust force obtained from experiment (RUN No.5401) and time history of loading used in the pipe whip analyses

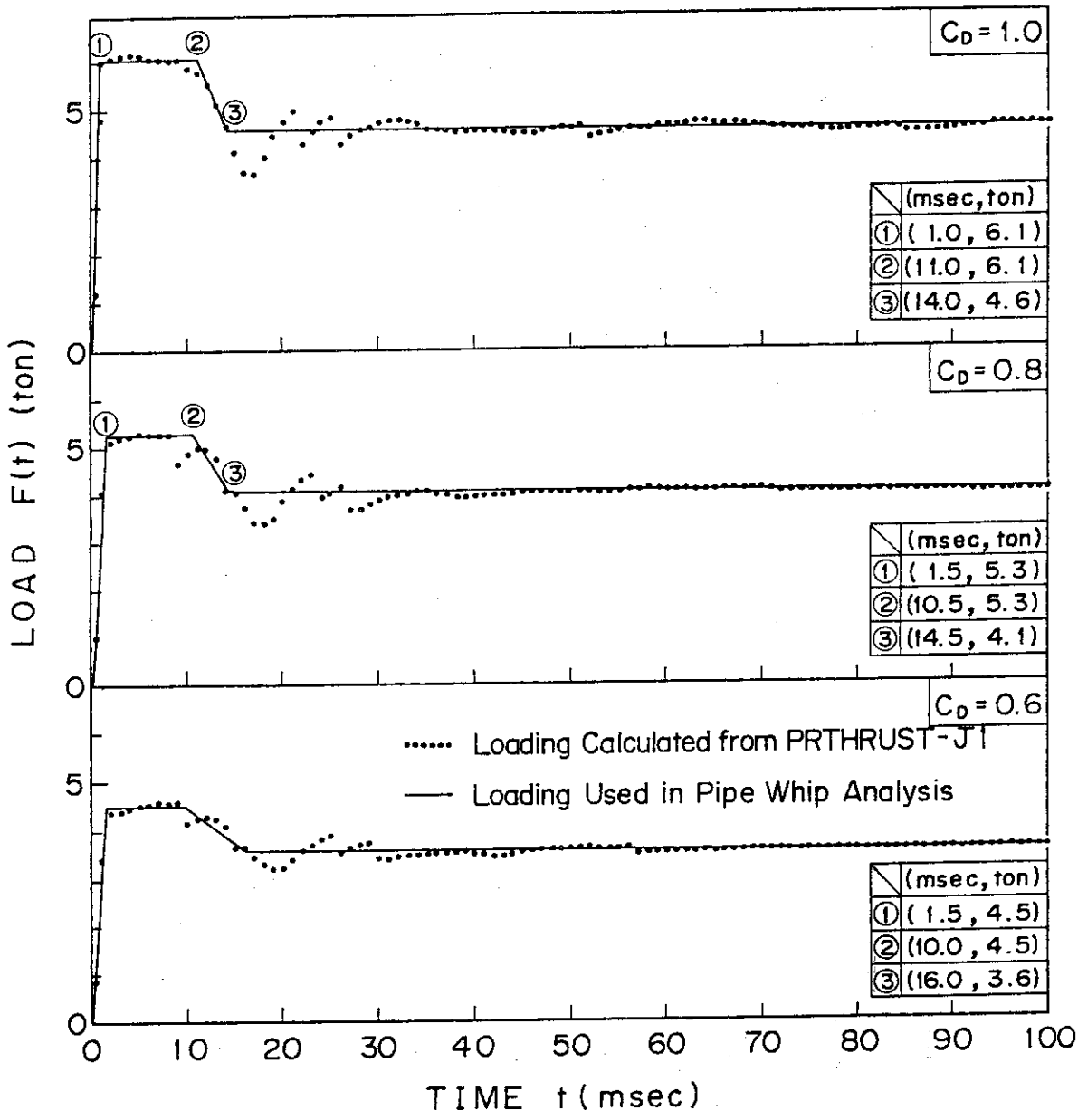

Fig. 5 Blowdown thrust force calculated by PRTHRUST-J1 code and time history of loading used in the pipe whip analyses

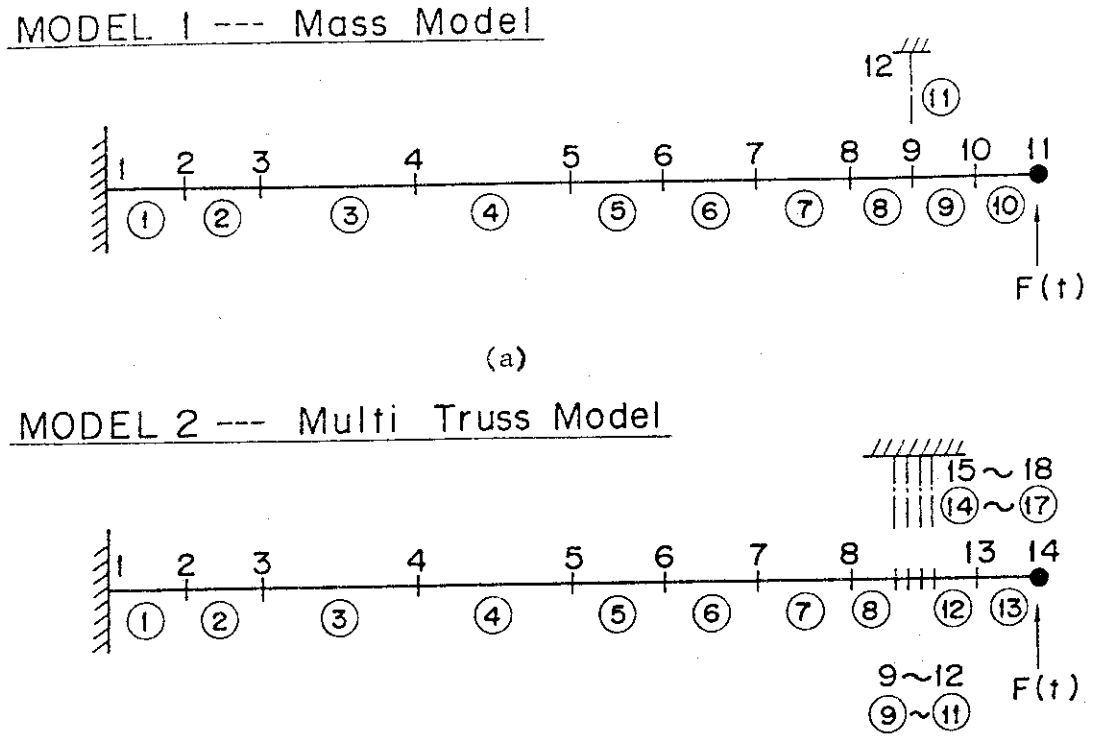

Fig. 6 Three analytical models used in the pipe whip analyses by ADINA code

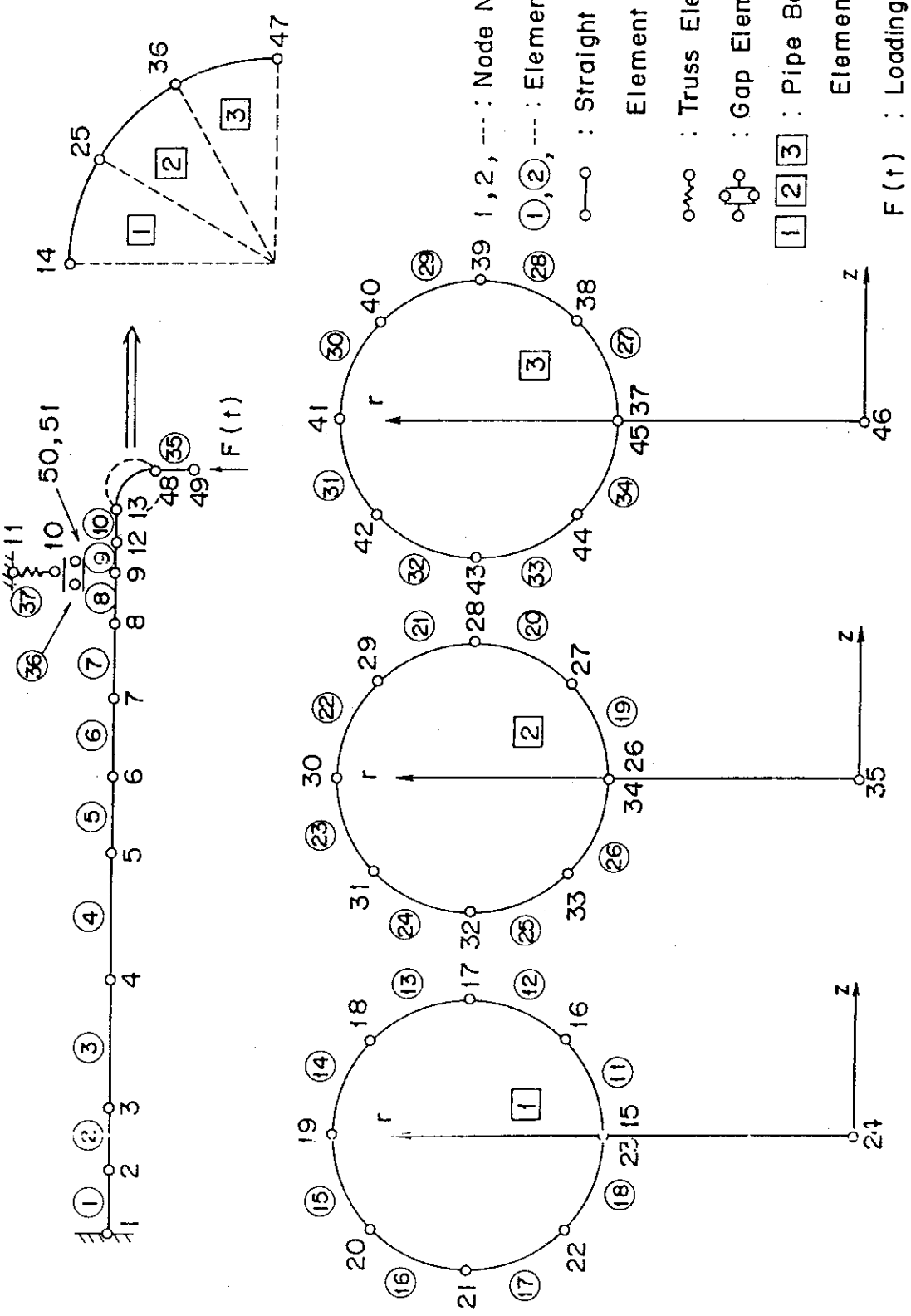

Fig. 7 Analytical model used in the pipe whip analyses by MARC code

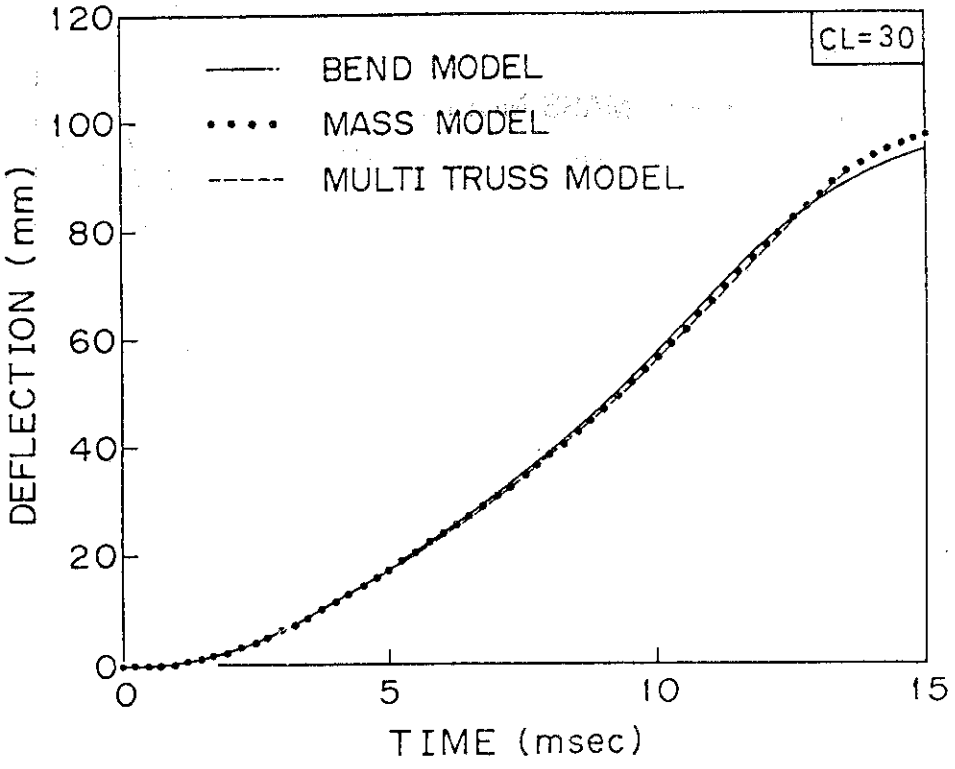

Fig. 8.1 Time history of pipe deflection at the loaded point--- Comparison among three models

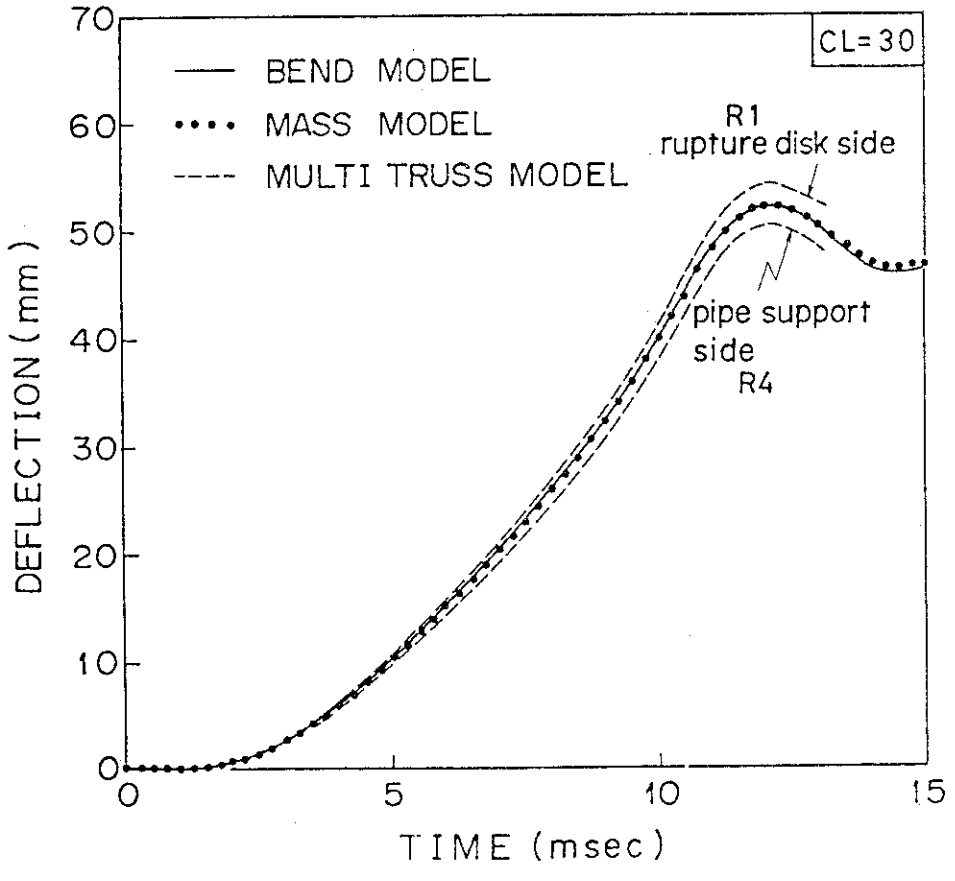

Fig. 8.2 Time history of pipe deflection at the restraint --- Comparison among three models

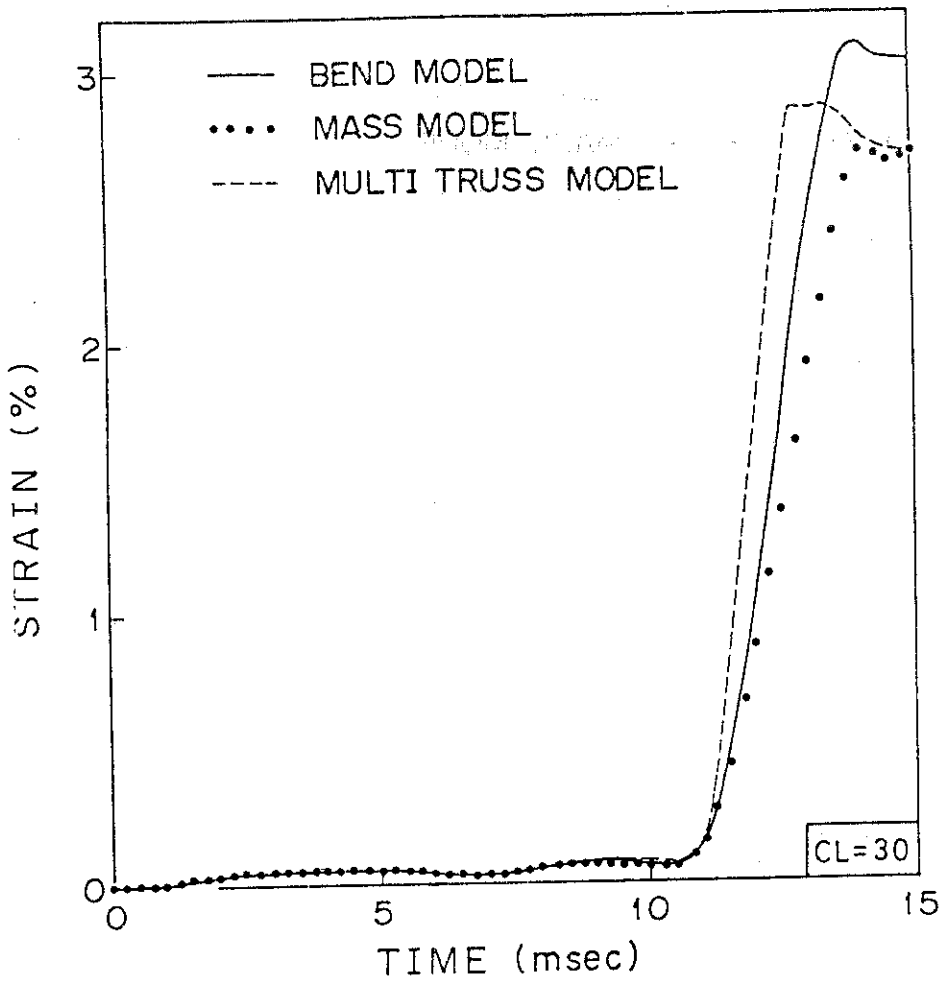

Fig. 8.3 Time history of fiber strain of the pipe at the restraint --- Comparison among three models

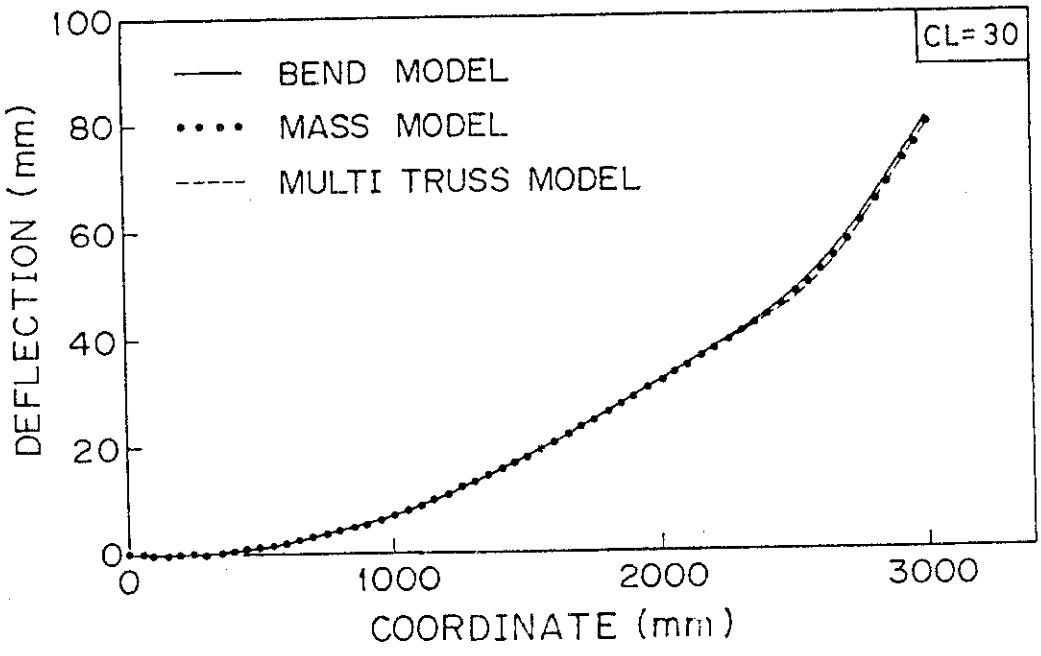

Fig. 8.5 Distribution of pipe deflection at the time when restraint displacement reaches maximum --- Comparison among three models

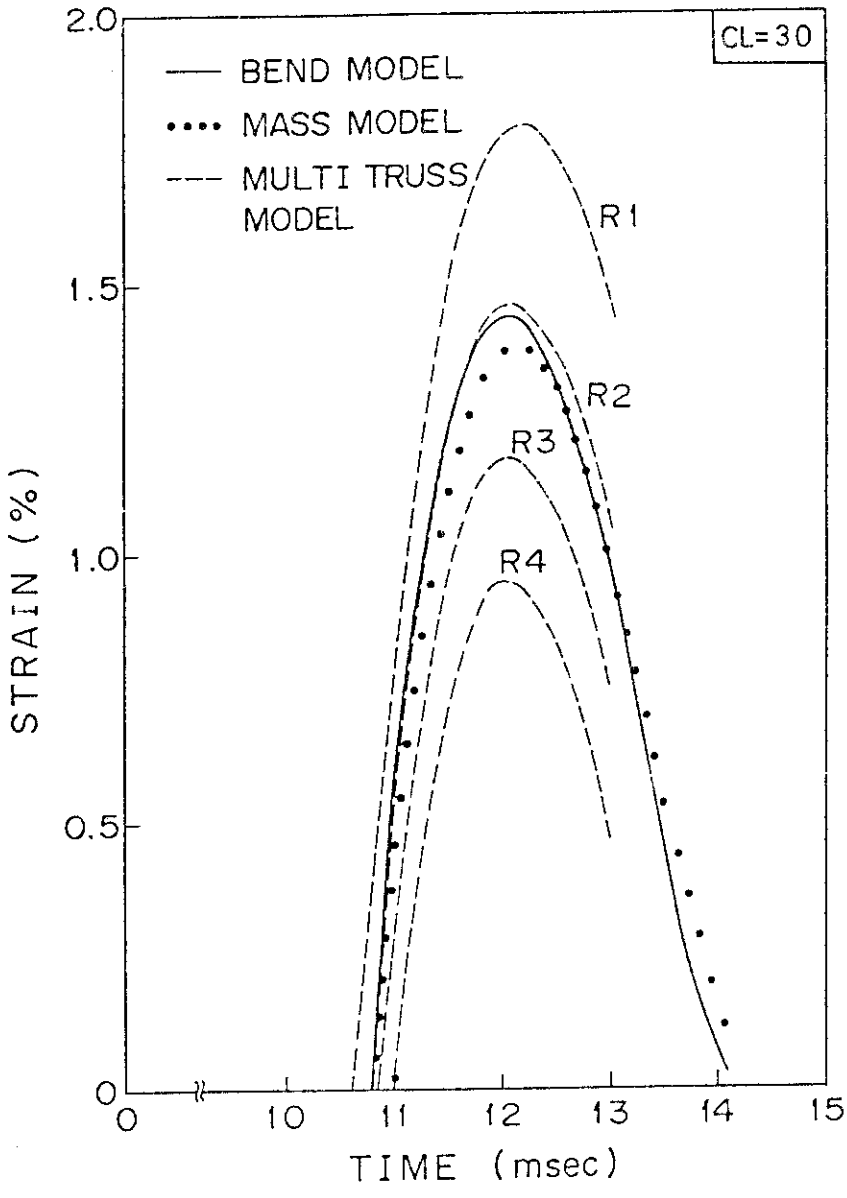

Fig. 8.4 Time history of restraint strain --- Comparison among three models

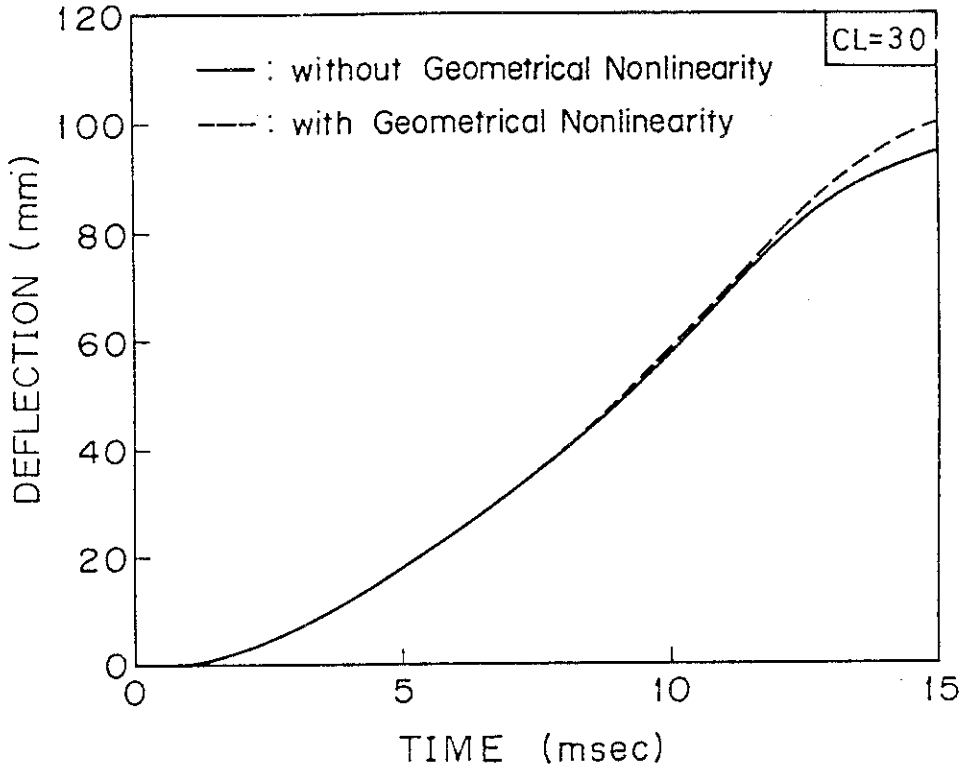

Fig. 9.1 Time history of pipe deflection at the loaded point --- Comparison between the analyses with and without geometrical nonlinearity

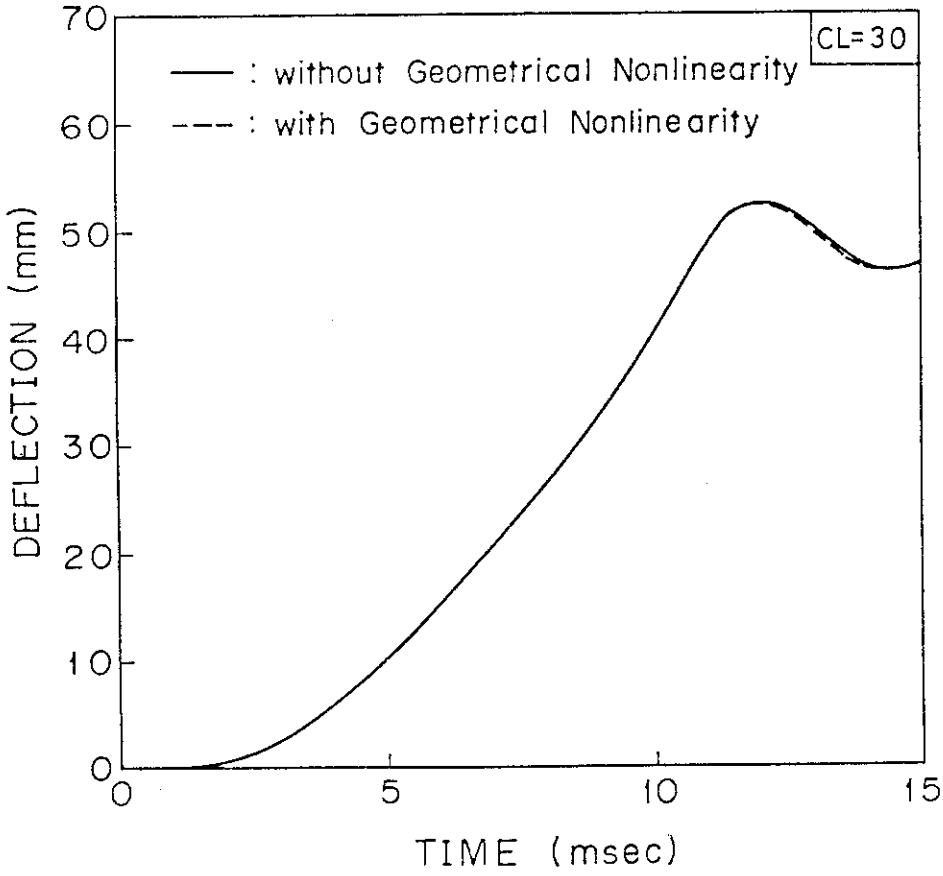

Fig. 9.2 Time history of pipe deflection at the restraint --- Comparison between the analyses with and without geometrical nonlinearity

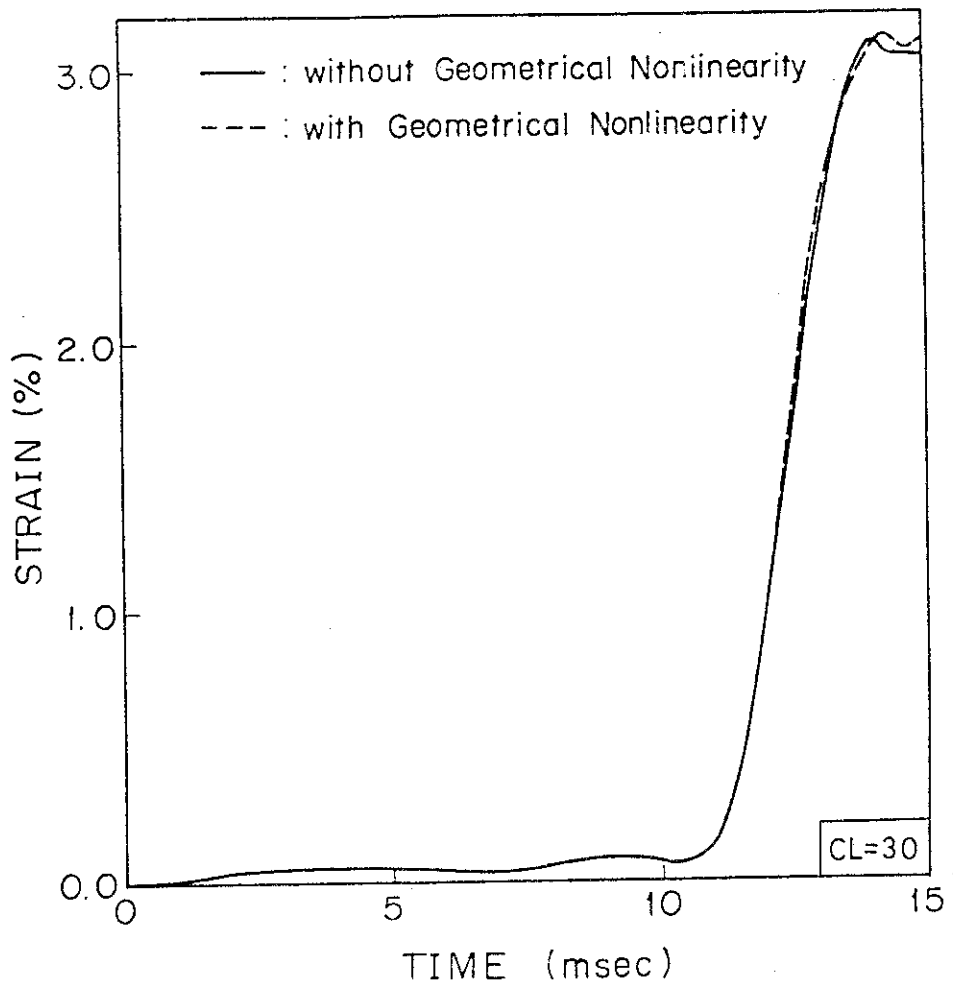

Fig. 9.3 Time history of fiber strain of pipe at the restraint --- Comparison between the analyses with and without geometrical nonlinearity

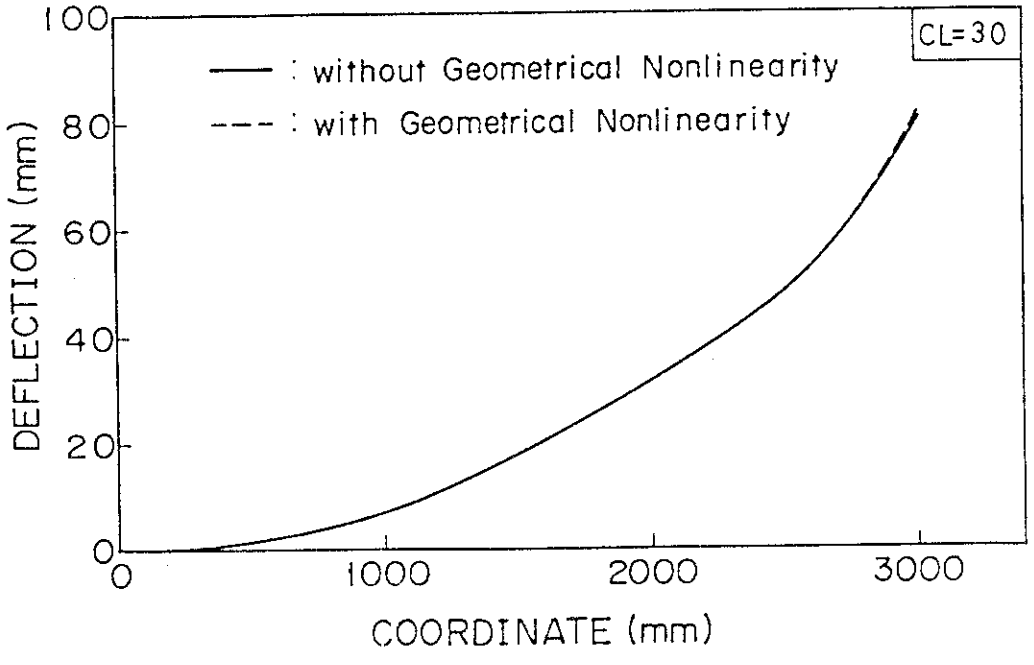

Fig. 9.5 Distribution of pipe deflection at the time when restraint displacement reaches maximum --- Comparison between the analyses with and without geometrical nonlinearity

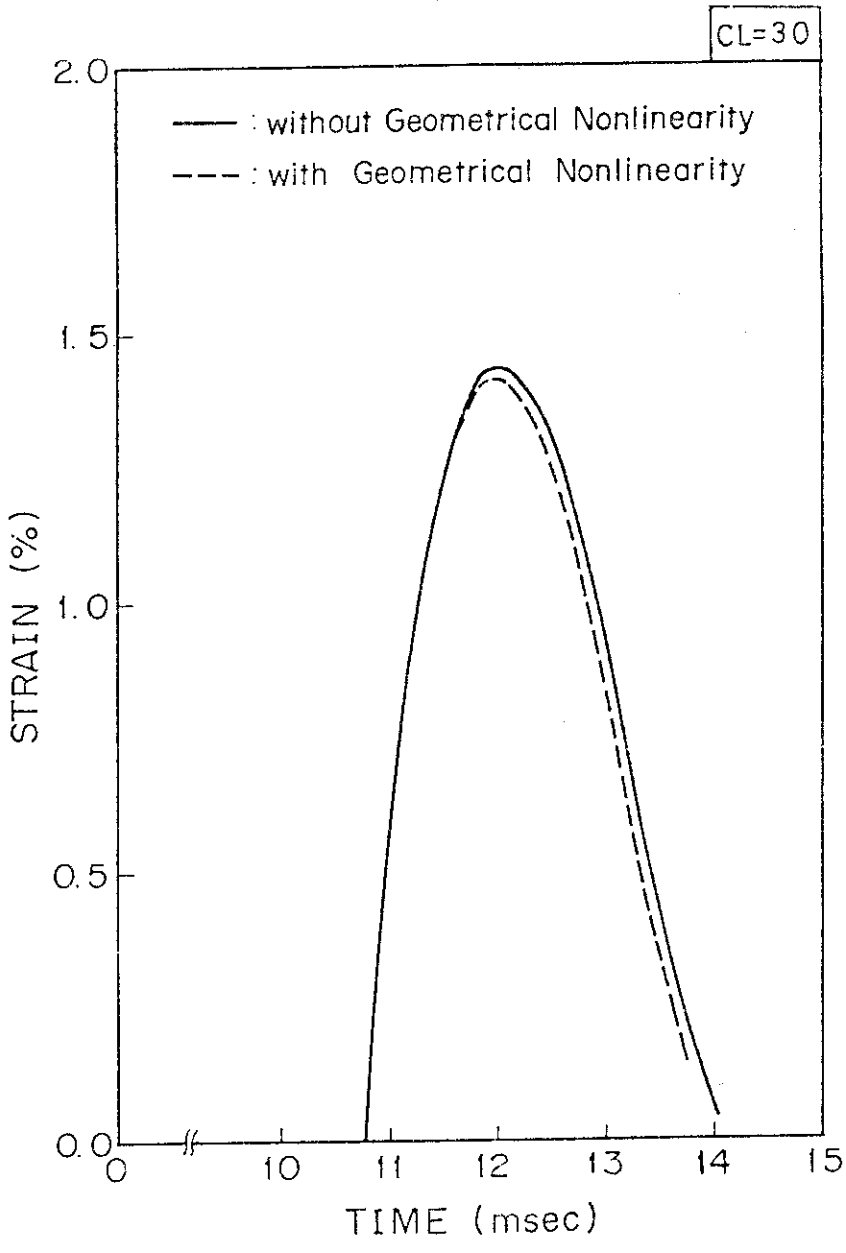

Fig. 9.4 Time history of restraint strain --- Comparison between the analysis with and without geometrical nonlinearity

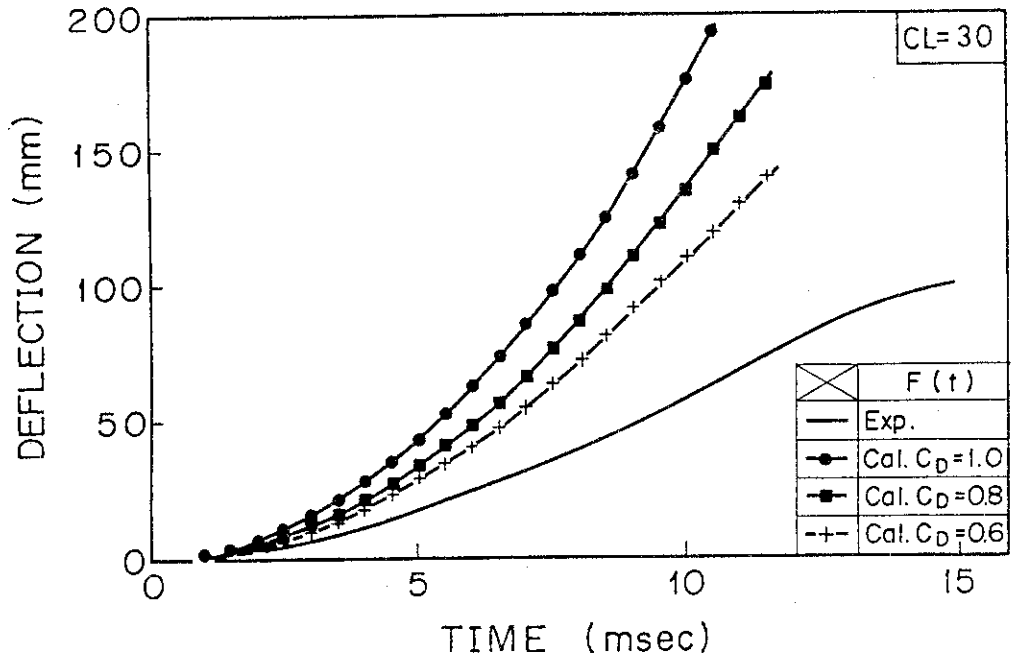

Fig. 10.1 Time history of pipe deflection at the loaded point (RUN No. 5405, CL = 30 mm)

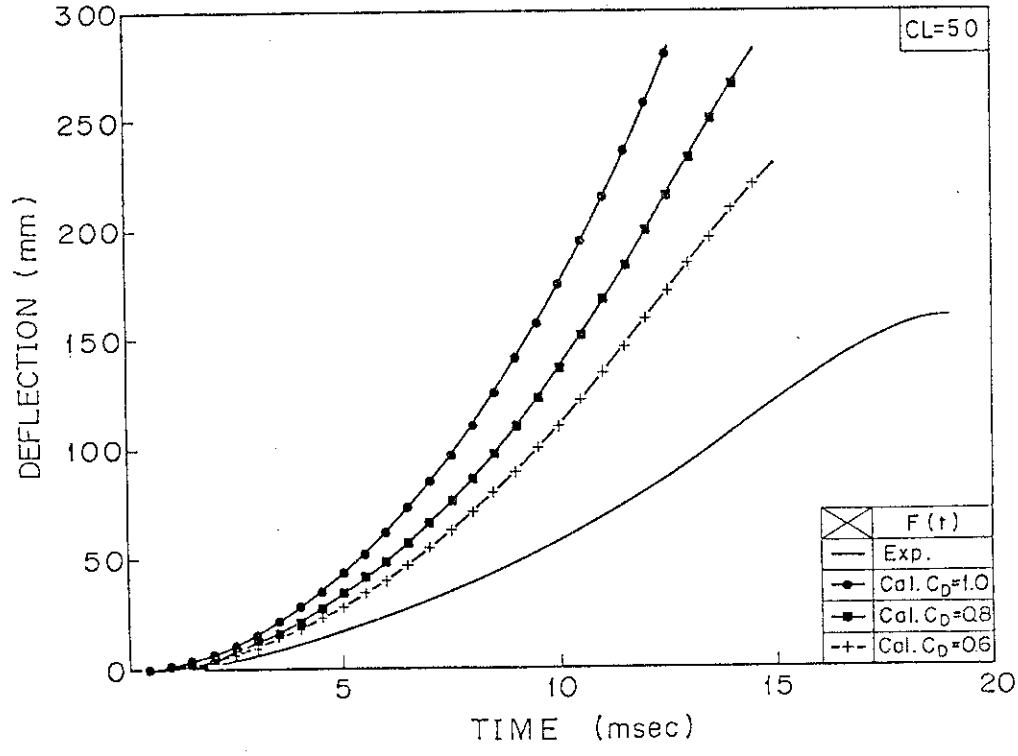

Fig. 10.2 Time history of pipe deflection at the loaded point (RUN No. 5406, CL = 50 mm)

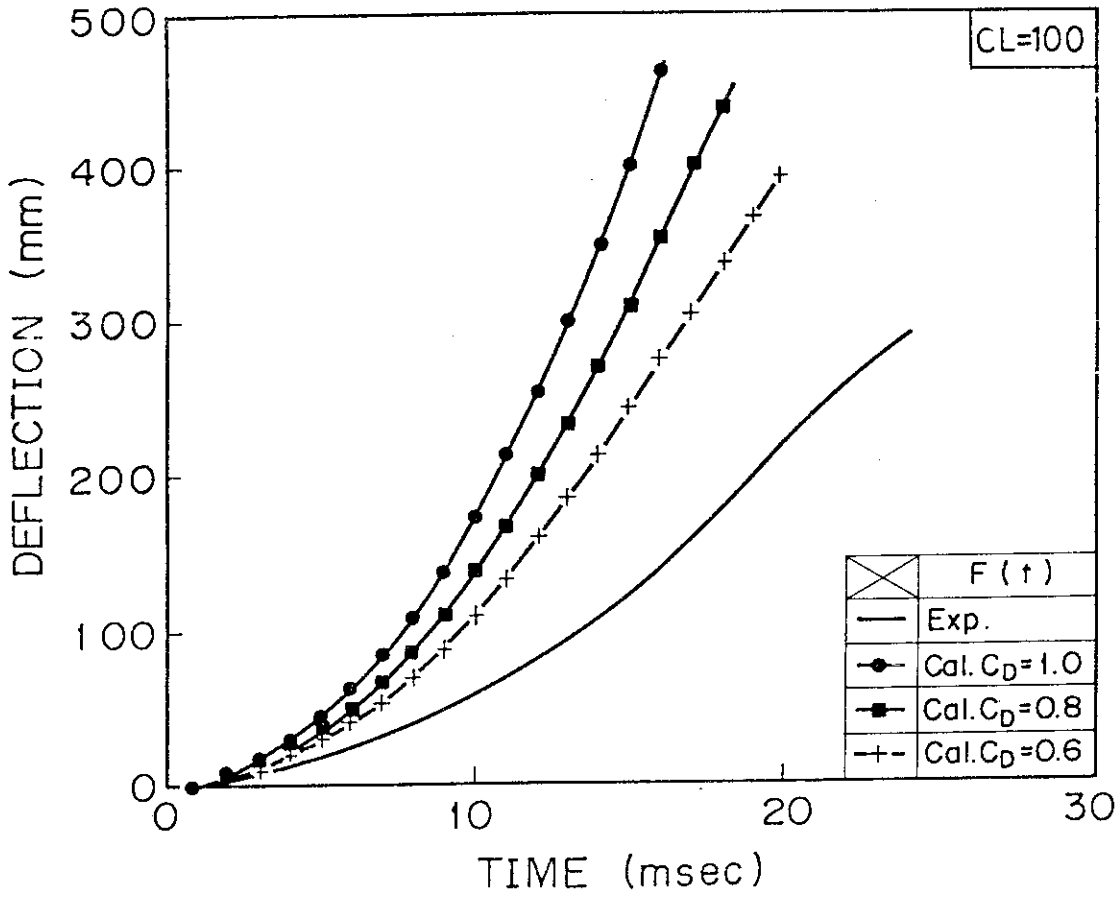

Fig. 10.3 Time history of pipe deflection at the loaded point (RUN No. 5407, CL = 100 mm)

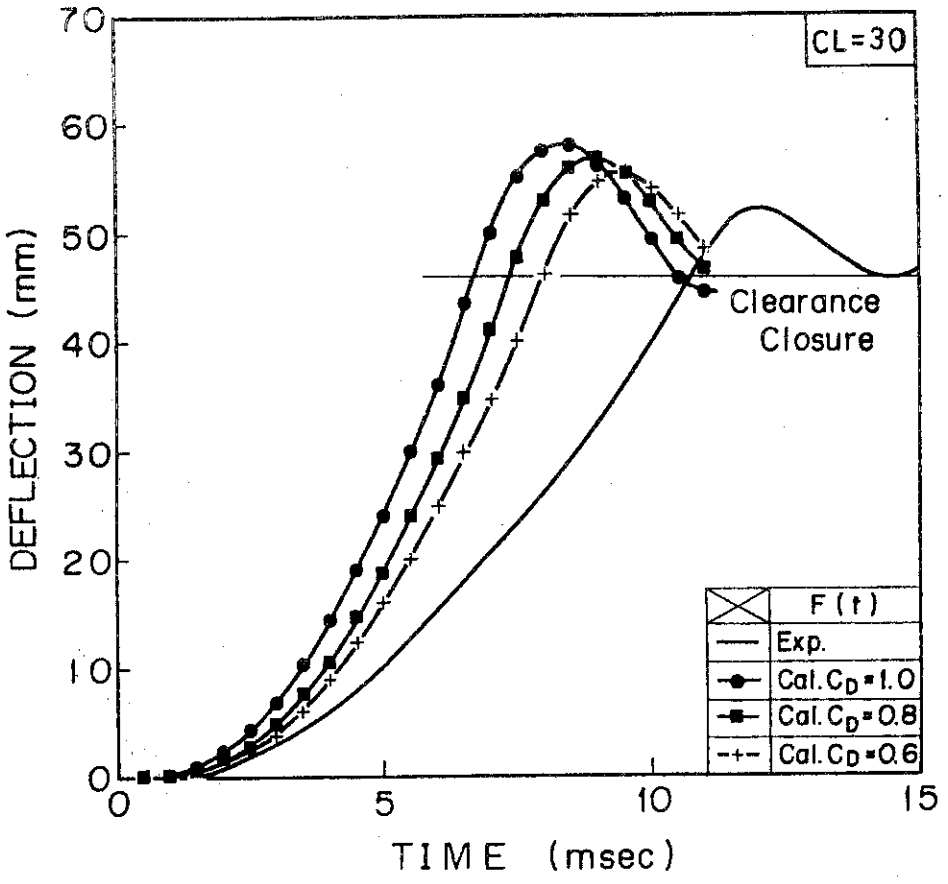

Fig.11.1 Time history of pipe deflection at restraint (RUN No.5405, CL=30mm)

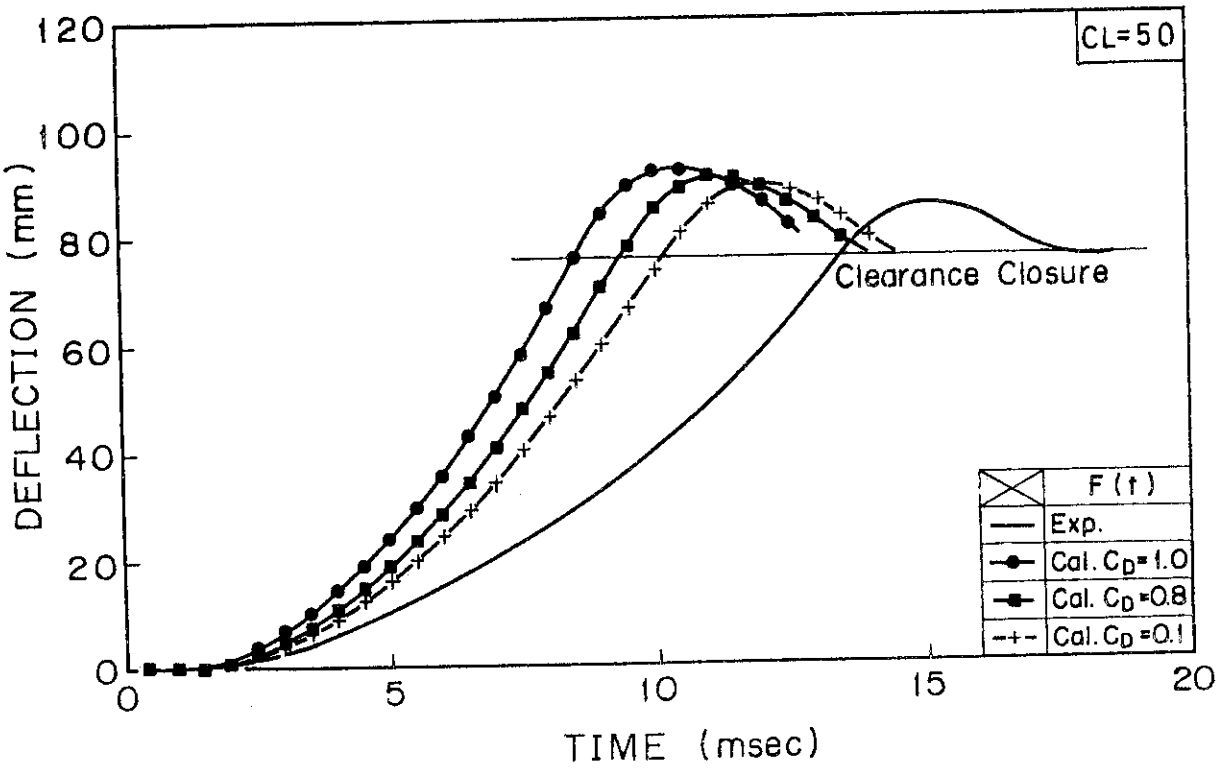

Fig.11.2 Time history of pipe deflection at restraint (RUN No.5406, CL=50mm)

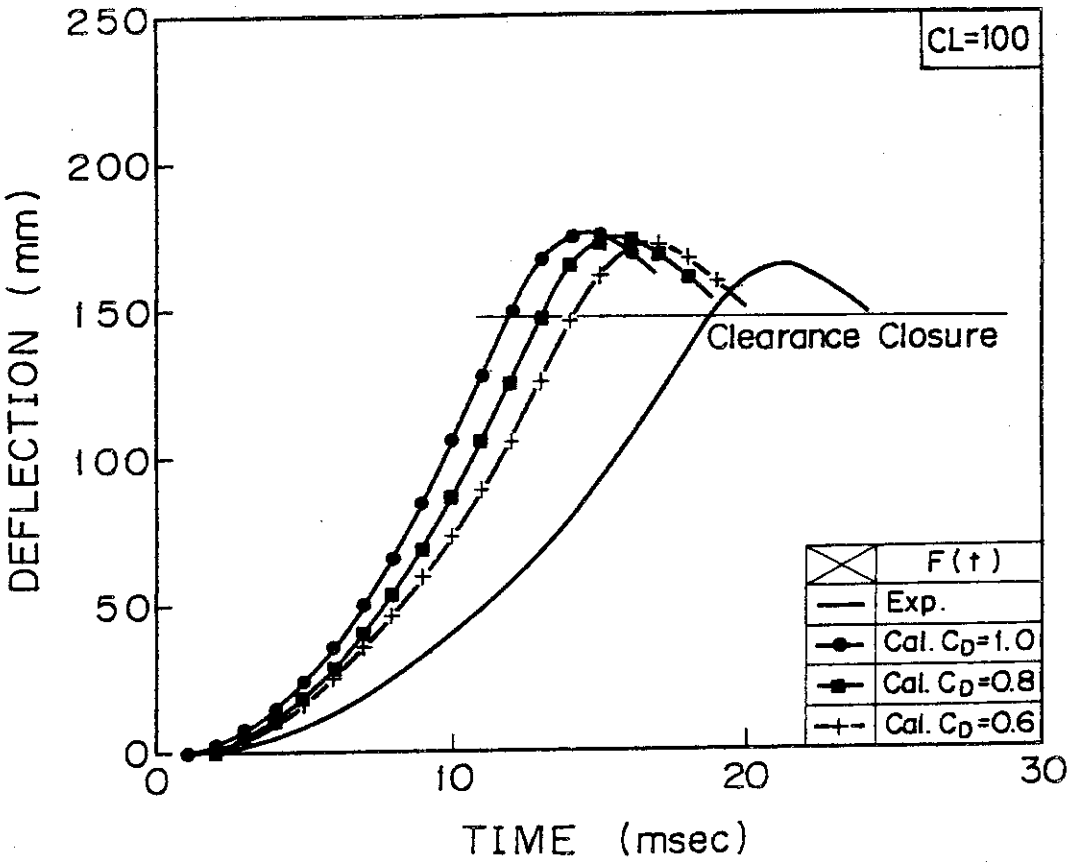

Fig. 11.3 Time history of pipe deflection at restraint (RUN No.5407, CL=100mm)

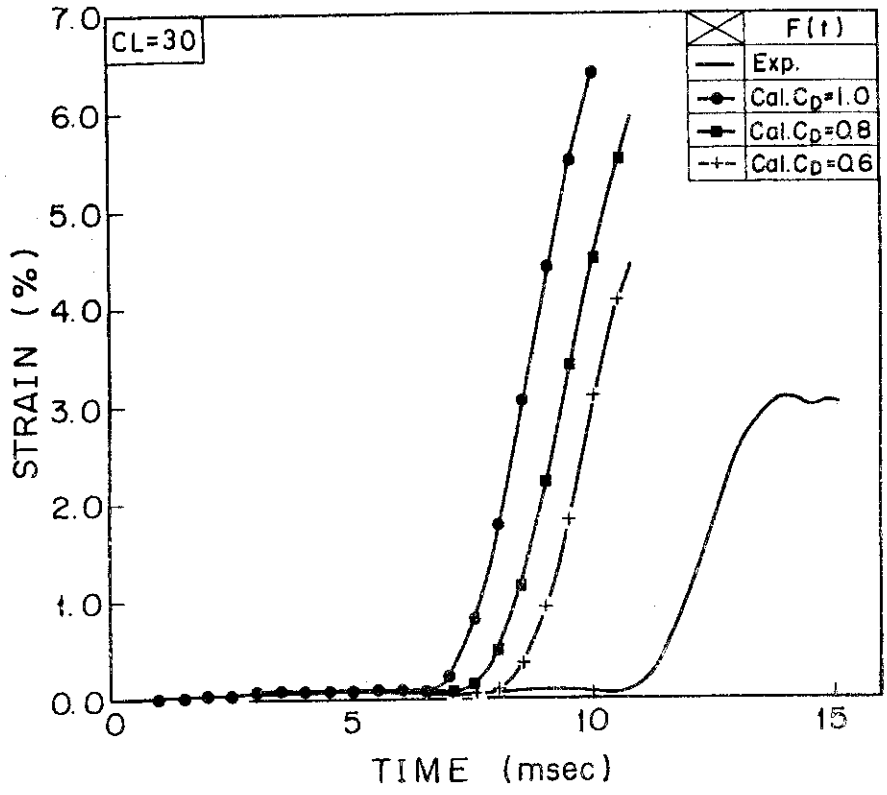

Fig. 12.1 Time history of fiber strain of pipe at restraint (RUN No.5405, CL=30mm)

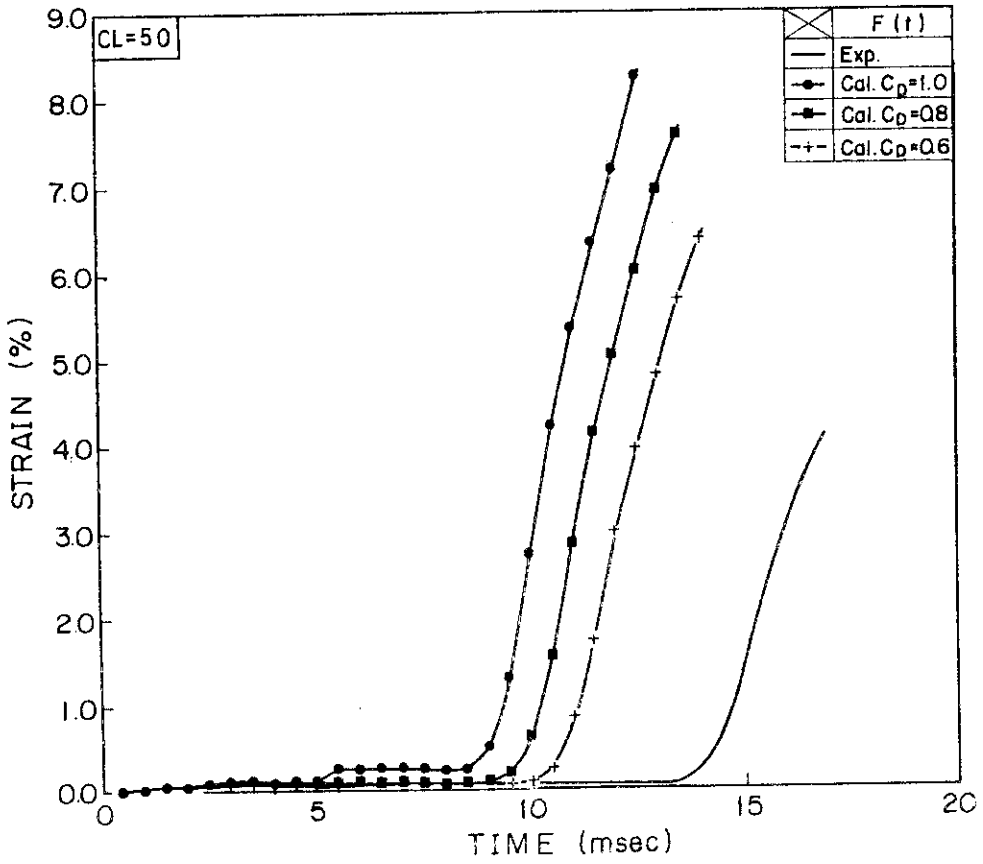

Fig. 12.2 Time history of fiber strain of pipe at restraint (RUN No.5406, CL=50mm)

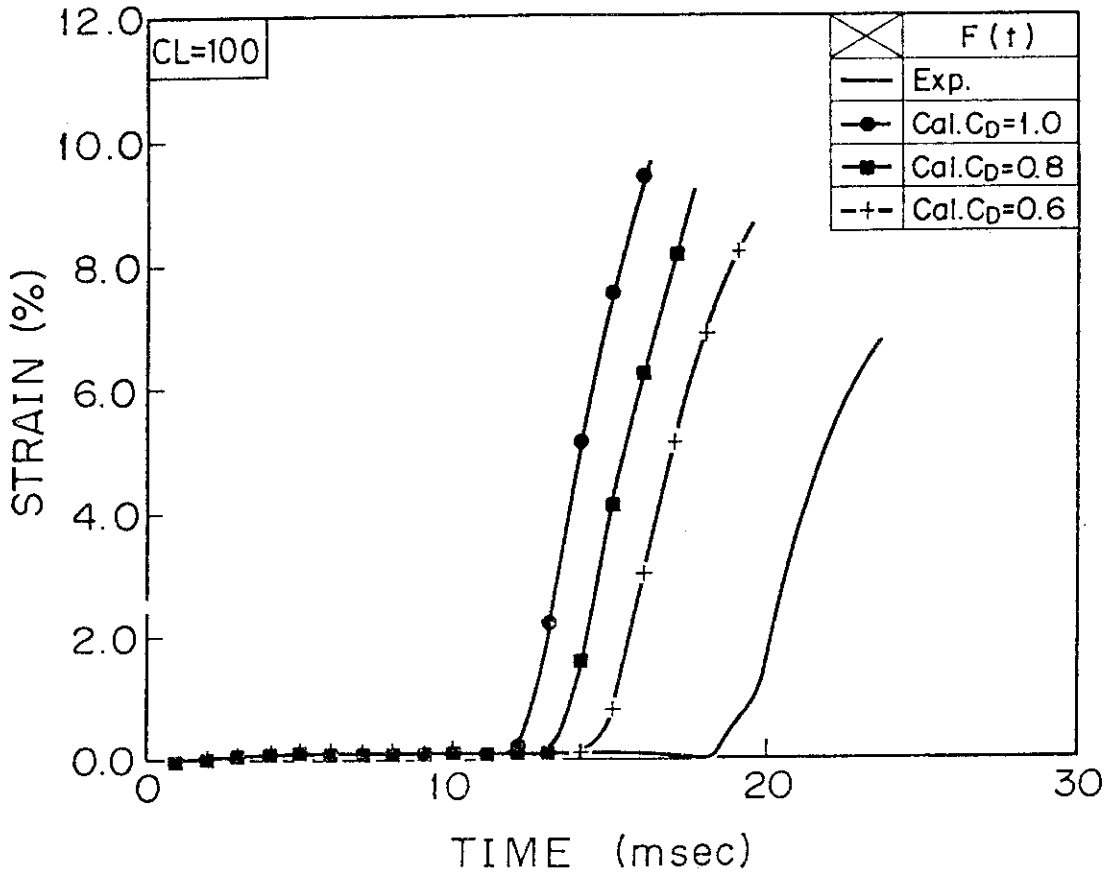

Fig. 12.3 Time history of fiber strain of pipe at restraint (RUN No.5407, CL=100mm)

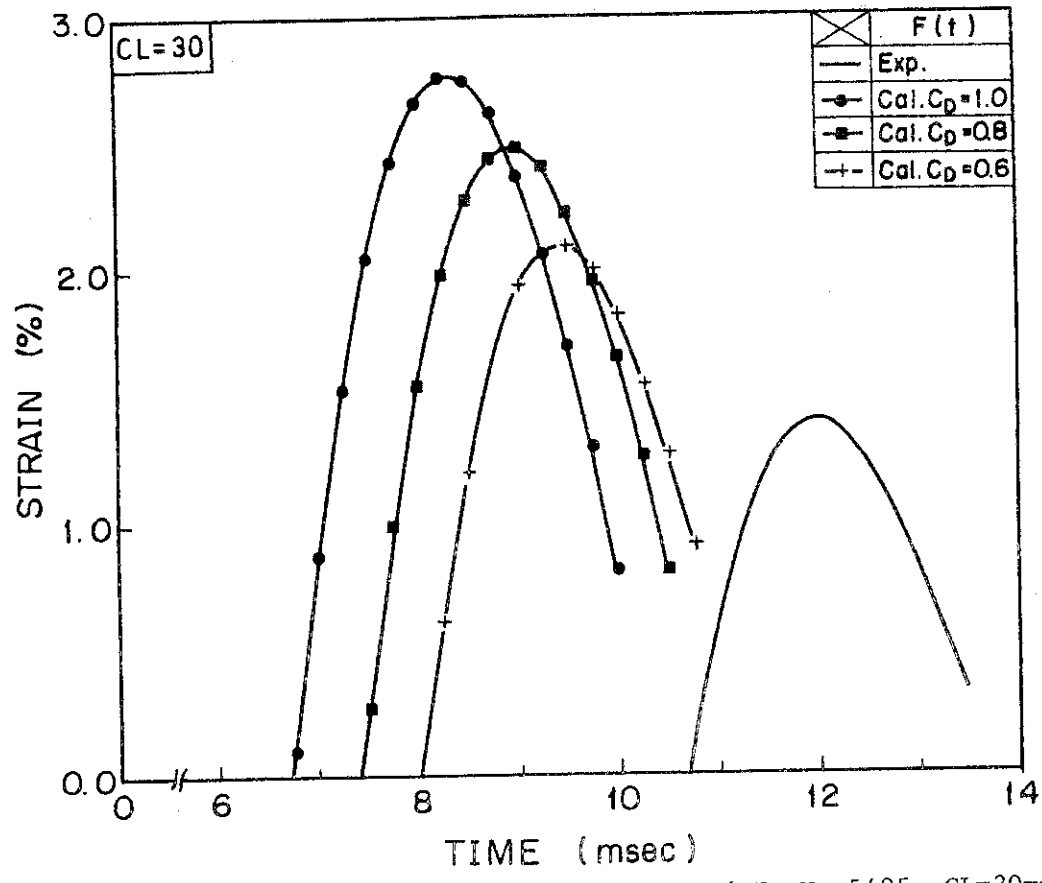

Fig.13.1 Time history of restraint strain (RUN No.5405, CL=30mm)

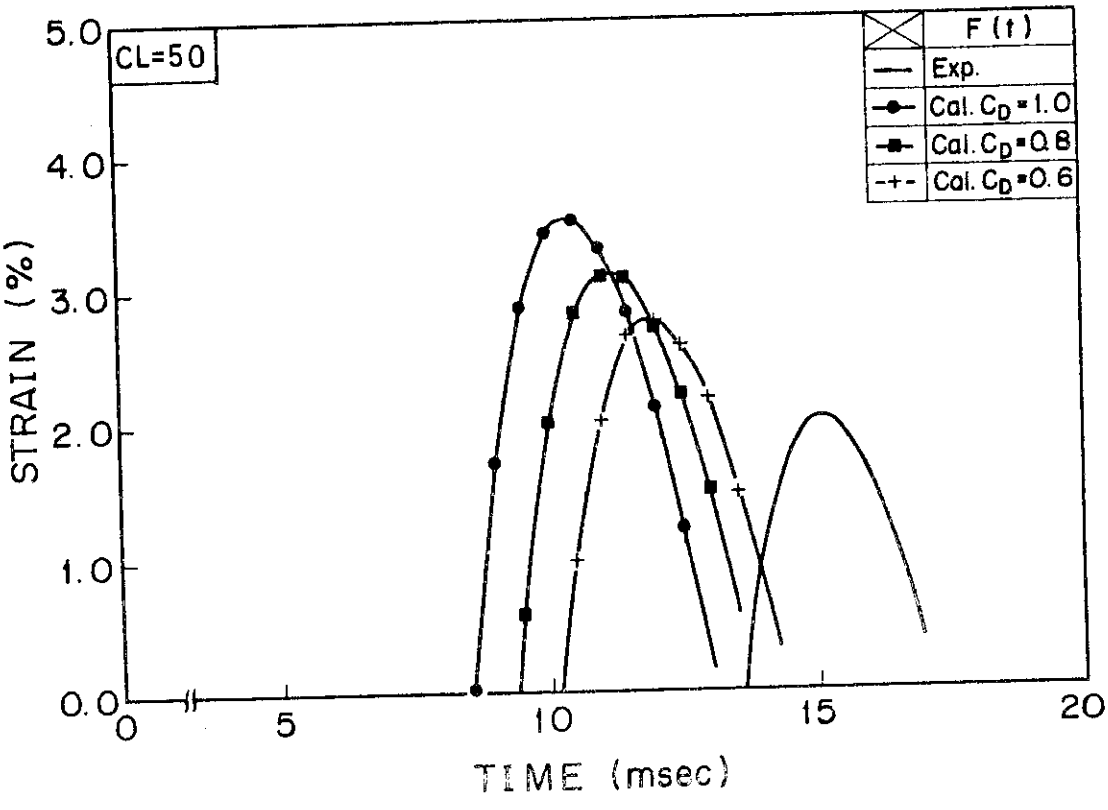

Fig.13.2 Time history of restraint strain (RUN No.5406, CL=50mm)

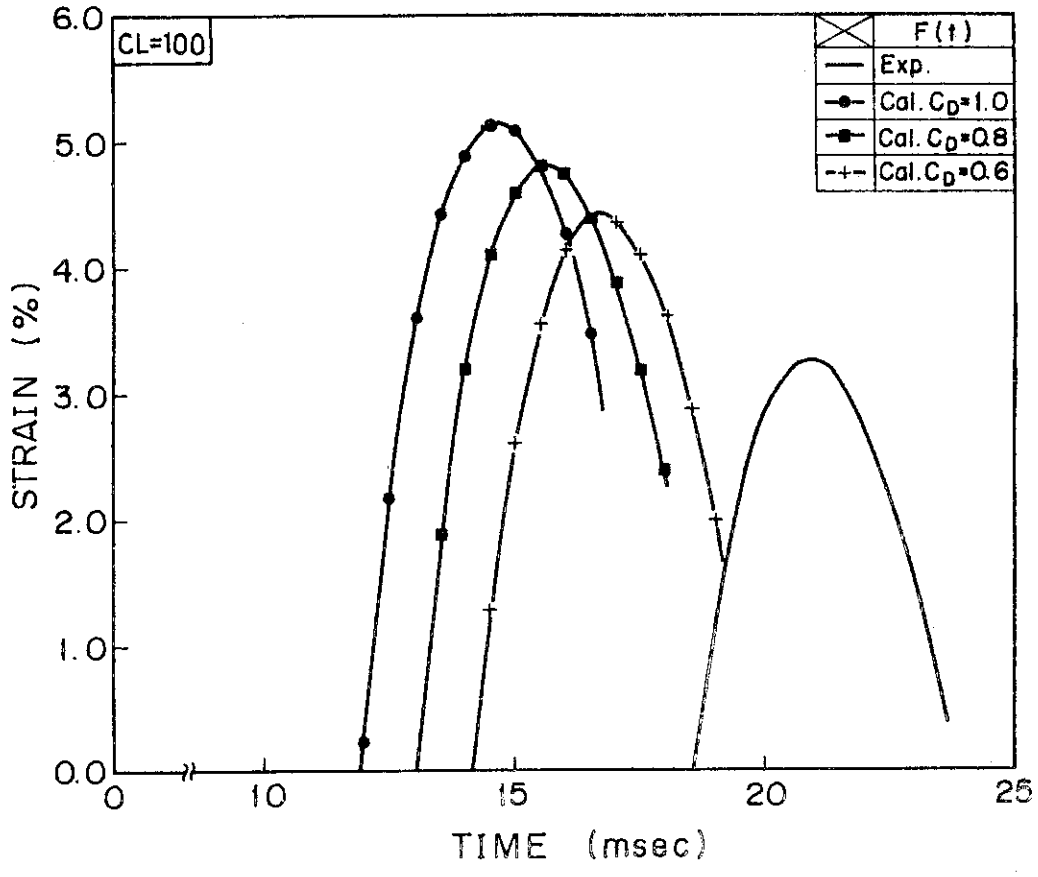

Fig.13.3 Time history of restraint strain (RUN No.5407, CL=100mm)

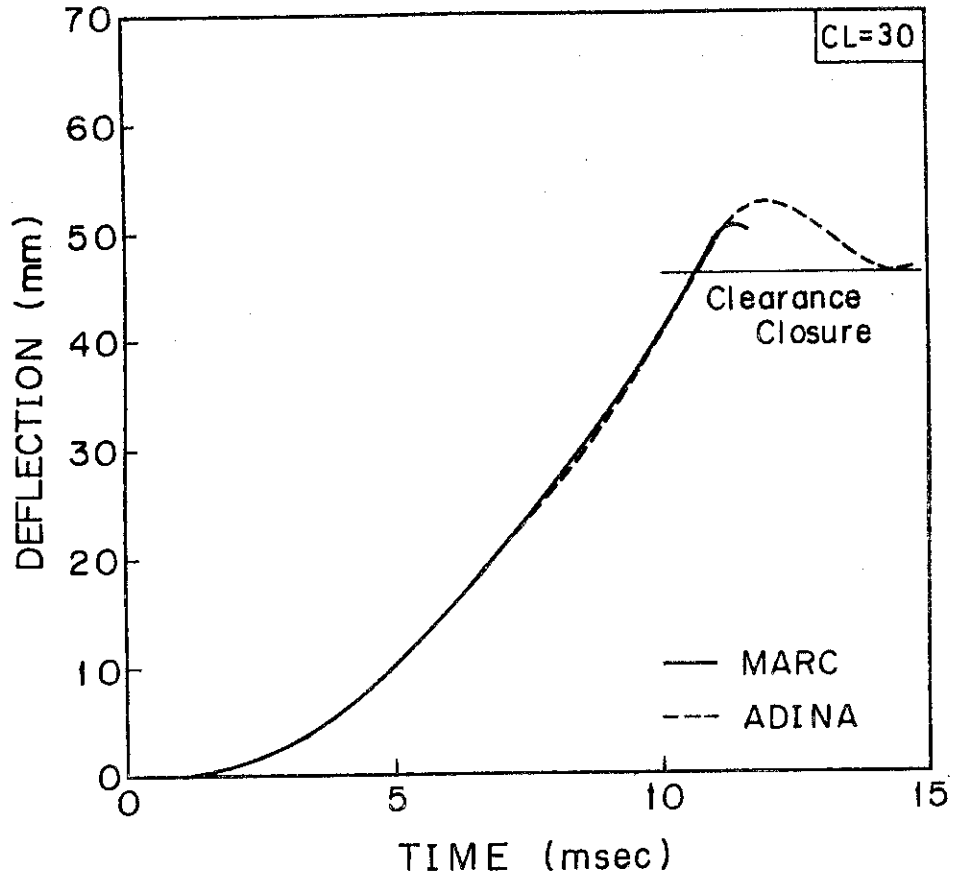

Fig.14.1 Time history of pipe deflection at restraint (RUN No.5405, CL=30mm) ----- Comparison between the results obtained by MARC and ADINA codes

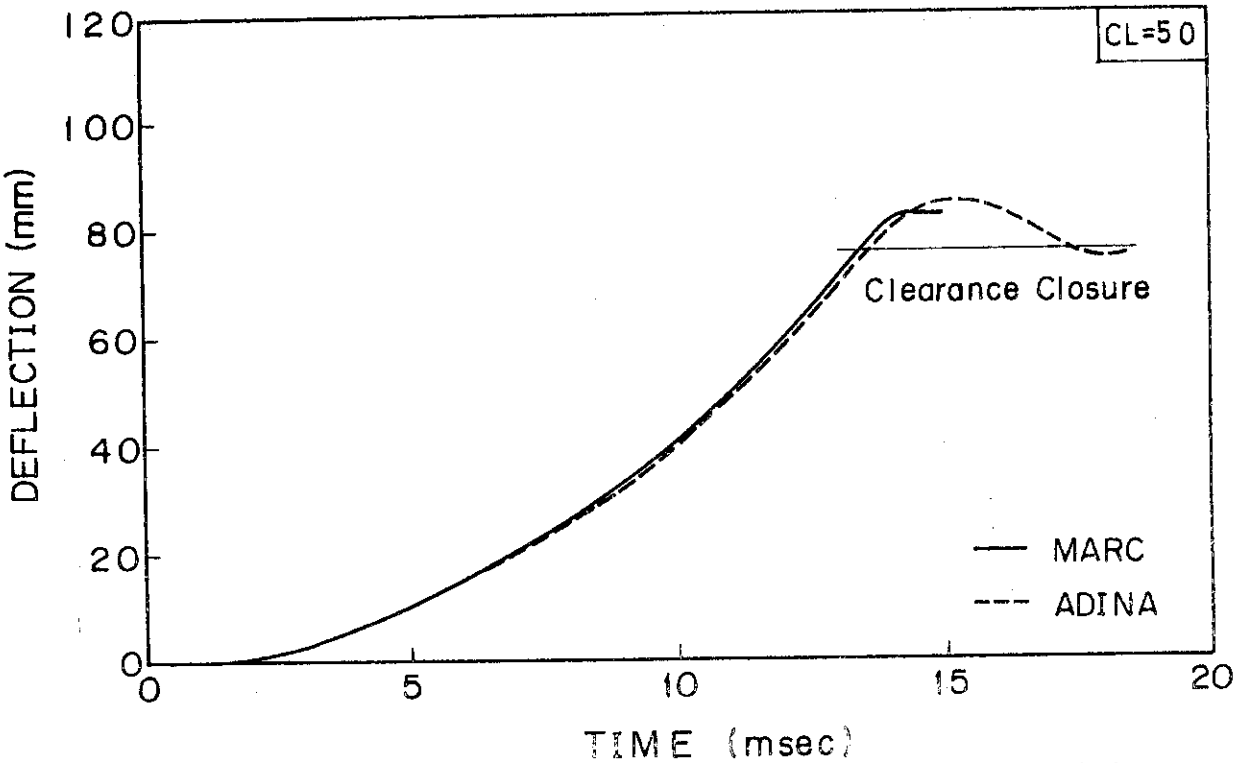

Fig.14.2 Time history of pipe deflection at restraint (RUN No.5406, CL=50mm) ----- Comparison between the results obtained by MARC and ADINA codes

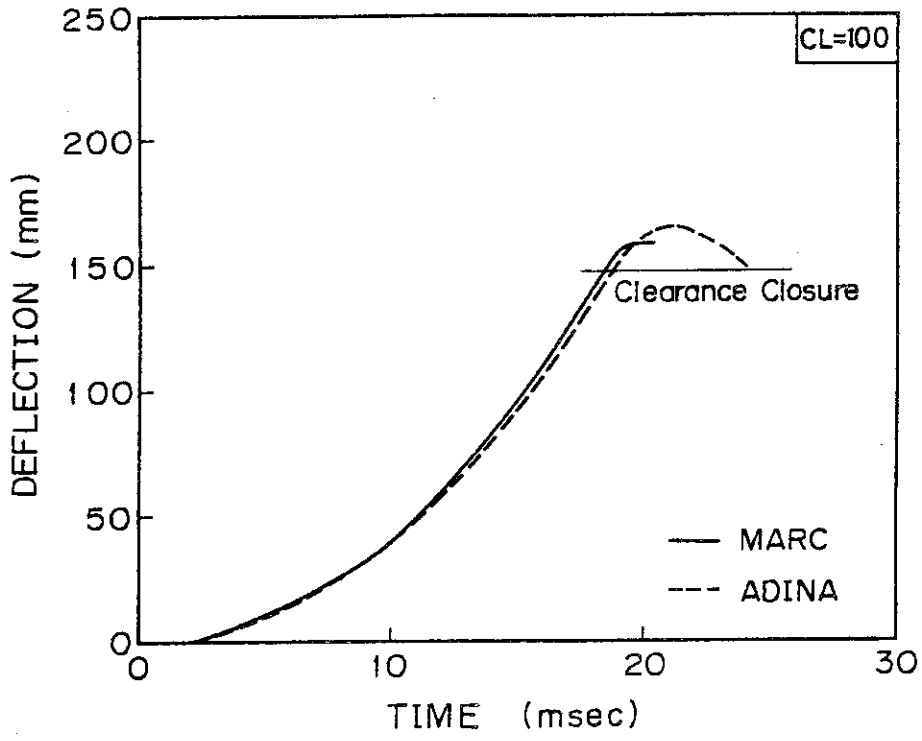

Fig. 14.3 Time history of pipe deflection at restraint (RUN No.5407, CL=100mm) ----- Comparison between the results obtained by MARC and ADINA codes

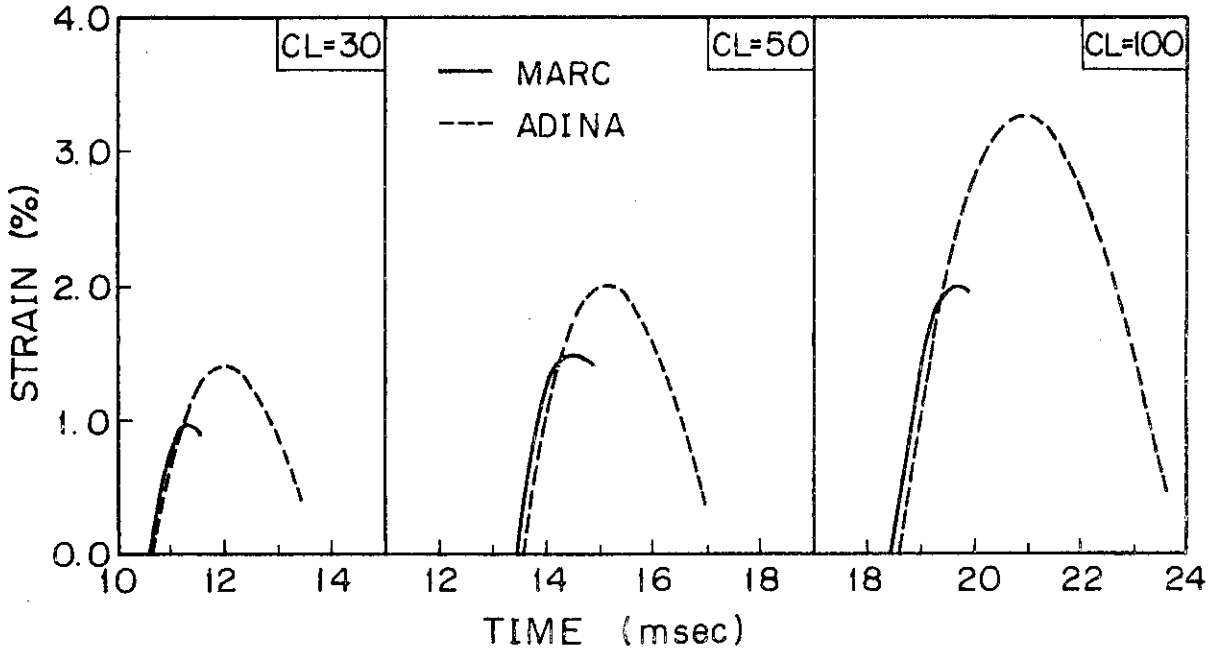

Fig. 15 Time history of restraint strain ----- Comparison between the results obtained by MARC and ADINA codes

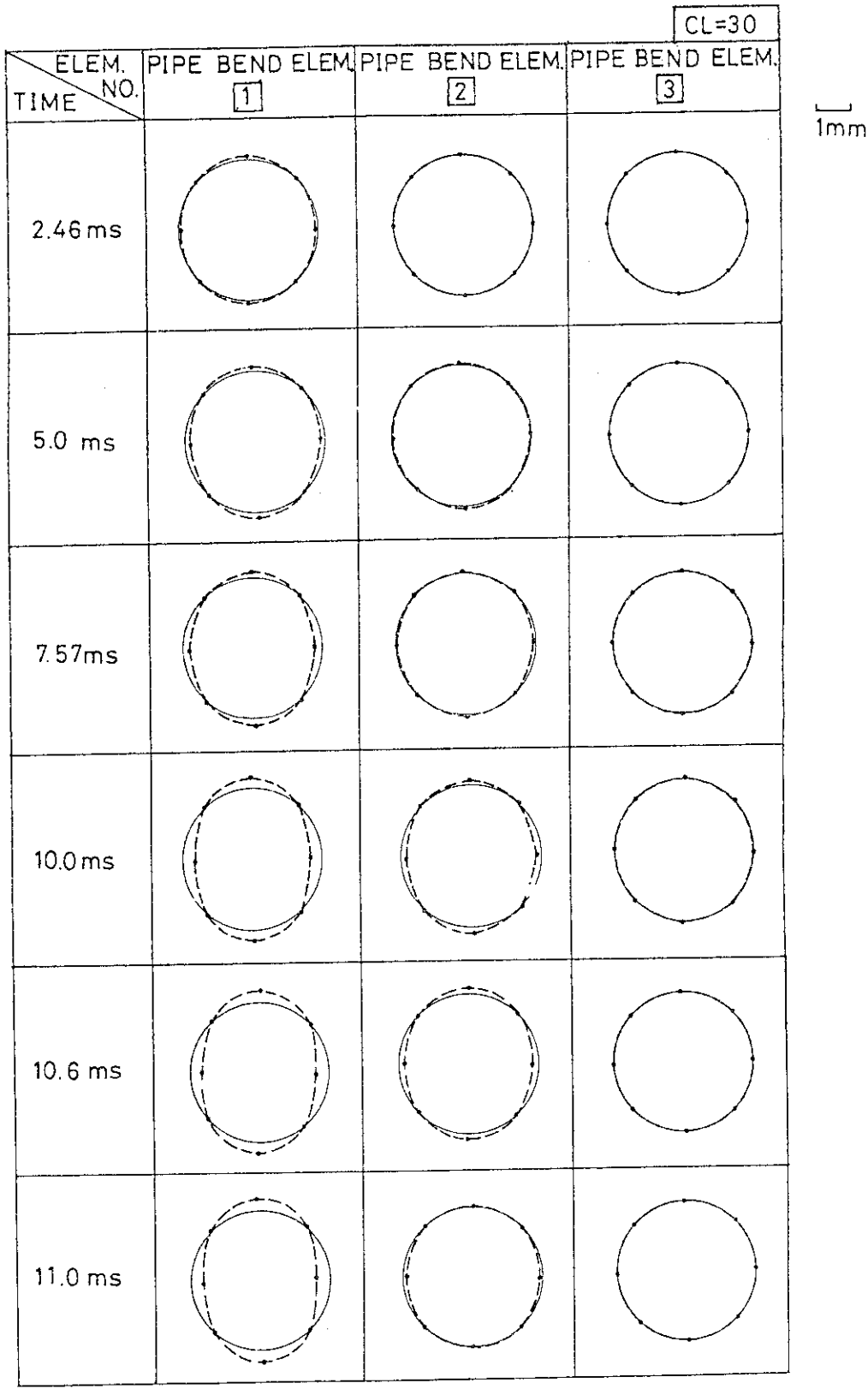

Fig. 16.1 Deformation of cross section in the elbow (RUN No.5405, CL=30mm) --- to be continued

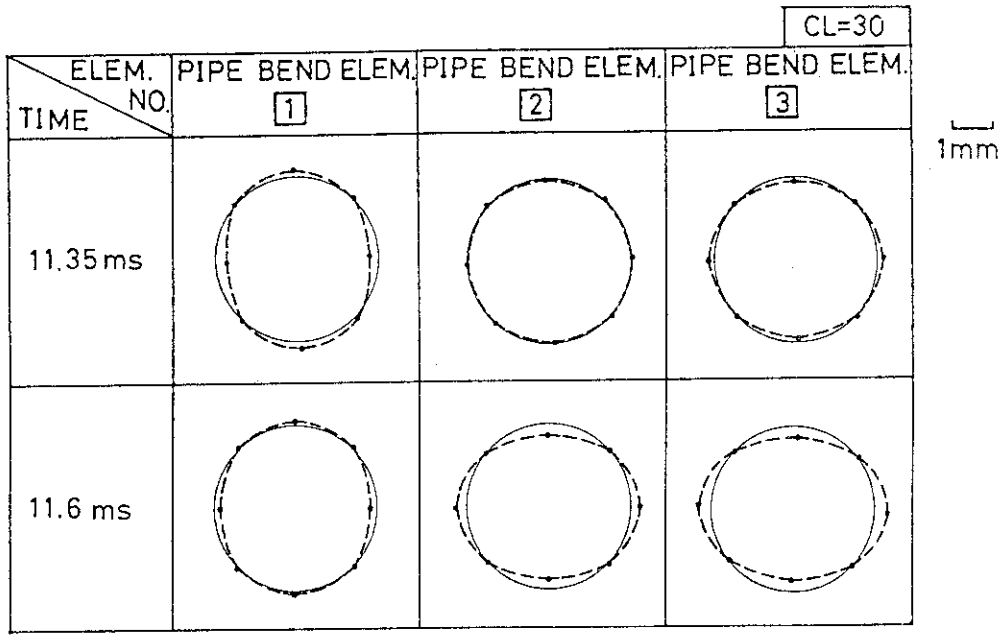

Fig. 16.1 Deformation of cross section in the elbow (RUN No.5405, CL=30mm)

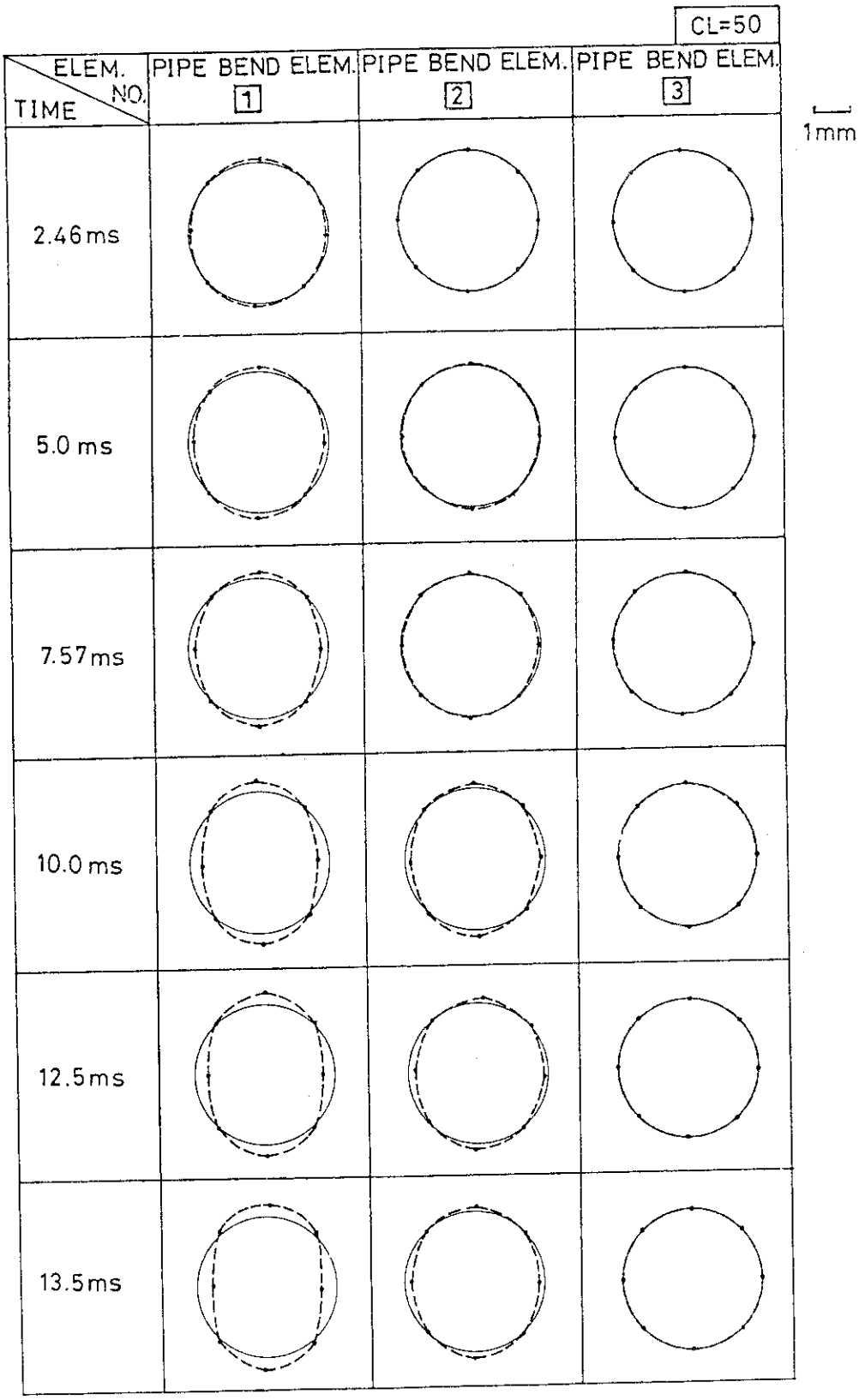

Fig. 16.2 Deformation of the cross section in the elbow (RUN No. 5406, CL = 50 mm) --- to be continued

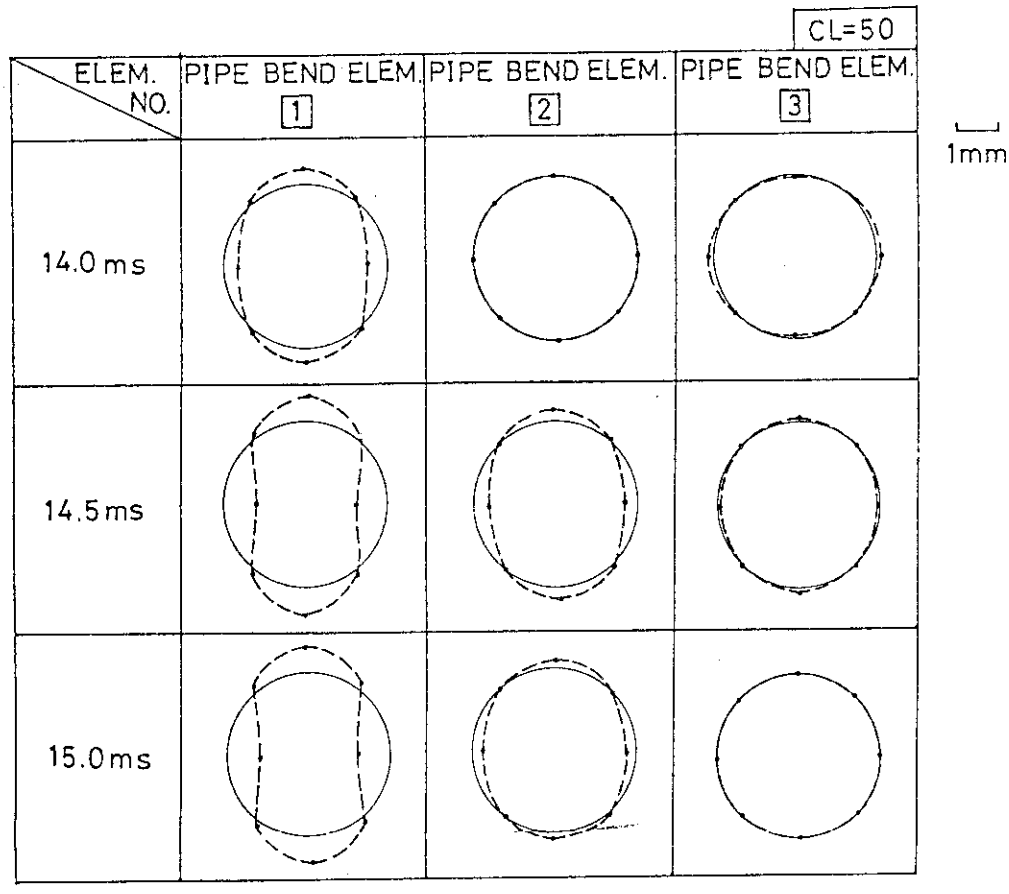

Fig. 16.2 Deformation of the cross section in the elbow (RUN No. 5406, CL = 50 mm)

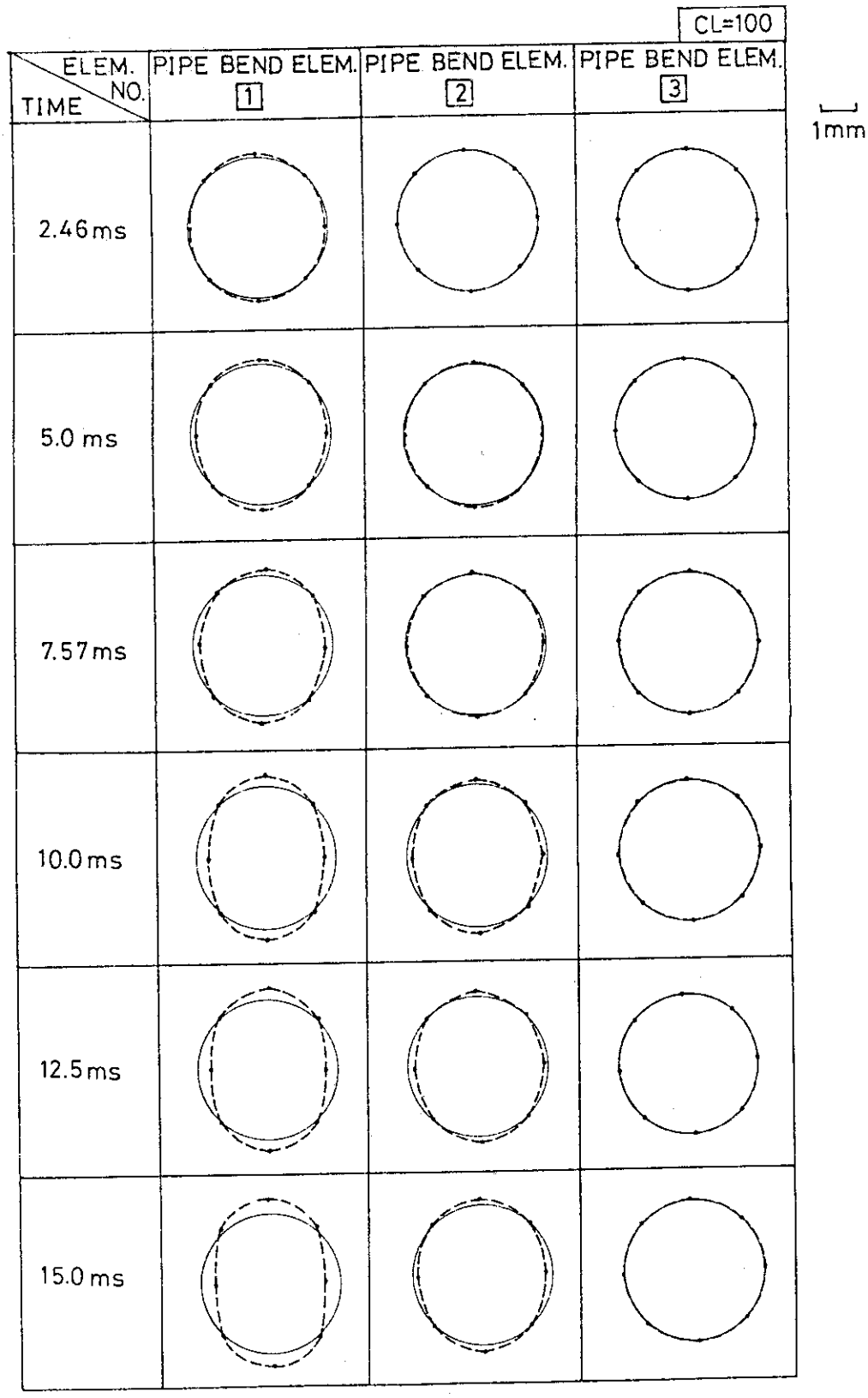

Fig. 16.3 Deformation of the cross section in the elbow (RUN No. 5407, CL = 100 mm) --- to be continued

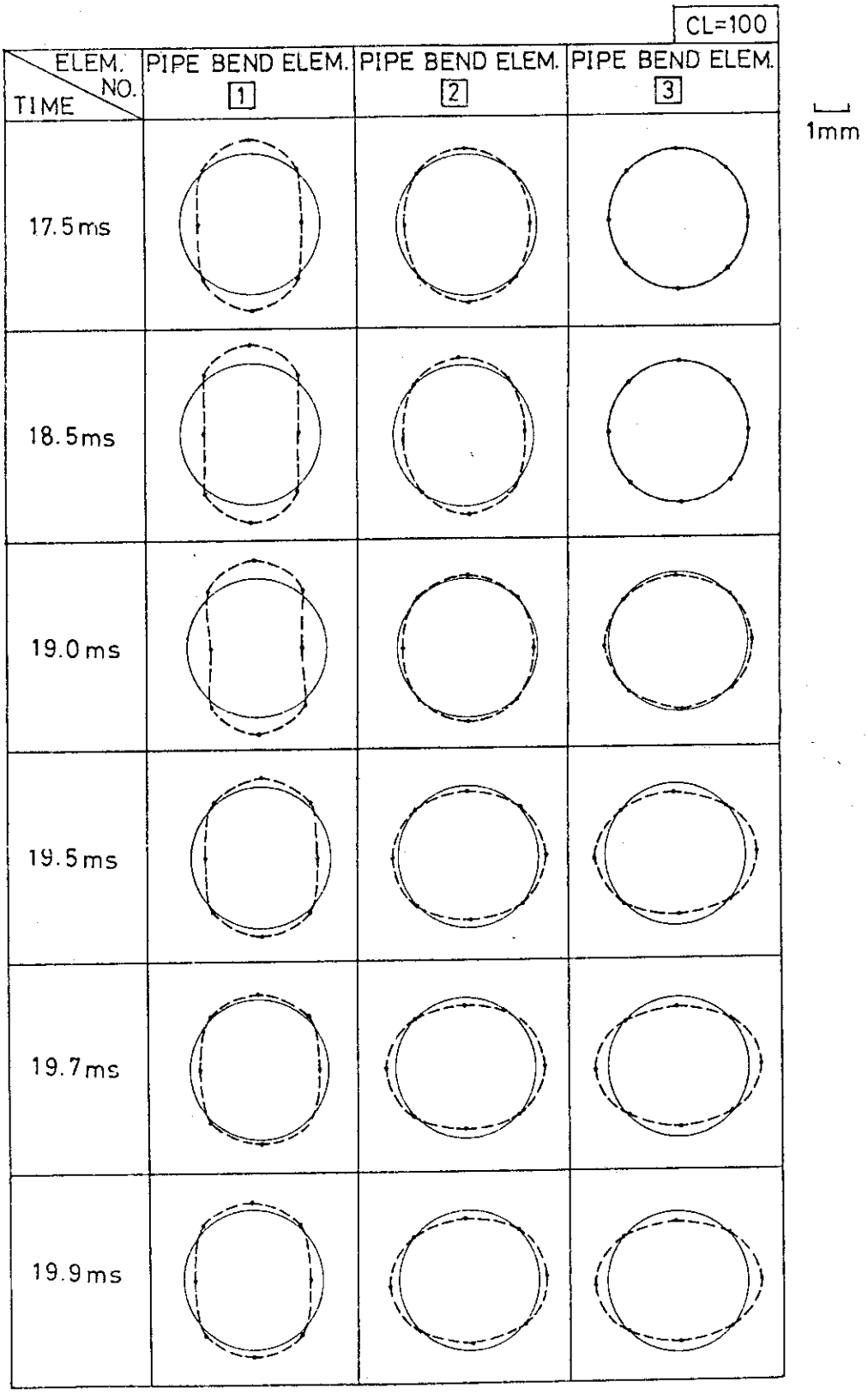

Fig. 16.3 Deformation of the cross section in the elbow (RUN No. 5407, CL = 100 mm)

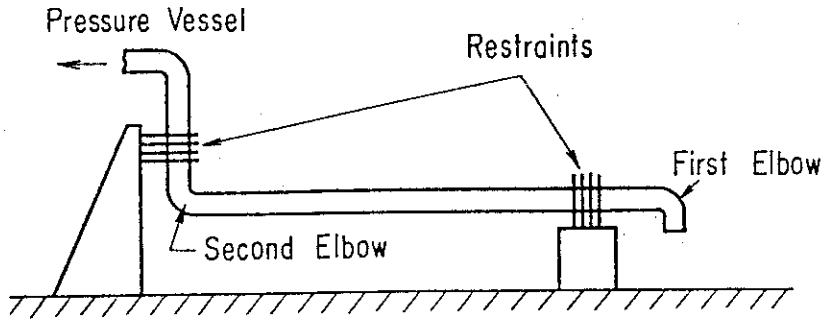

Fig. 17 The shell behavior should be considered in the second elbow in this figure

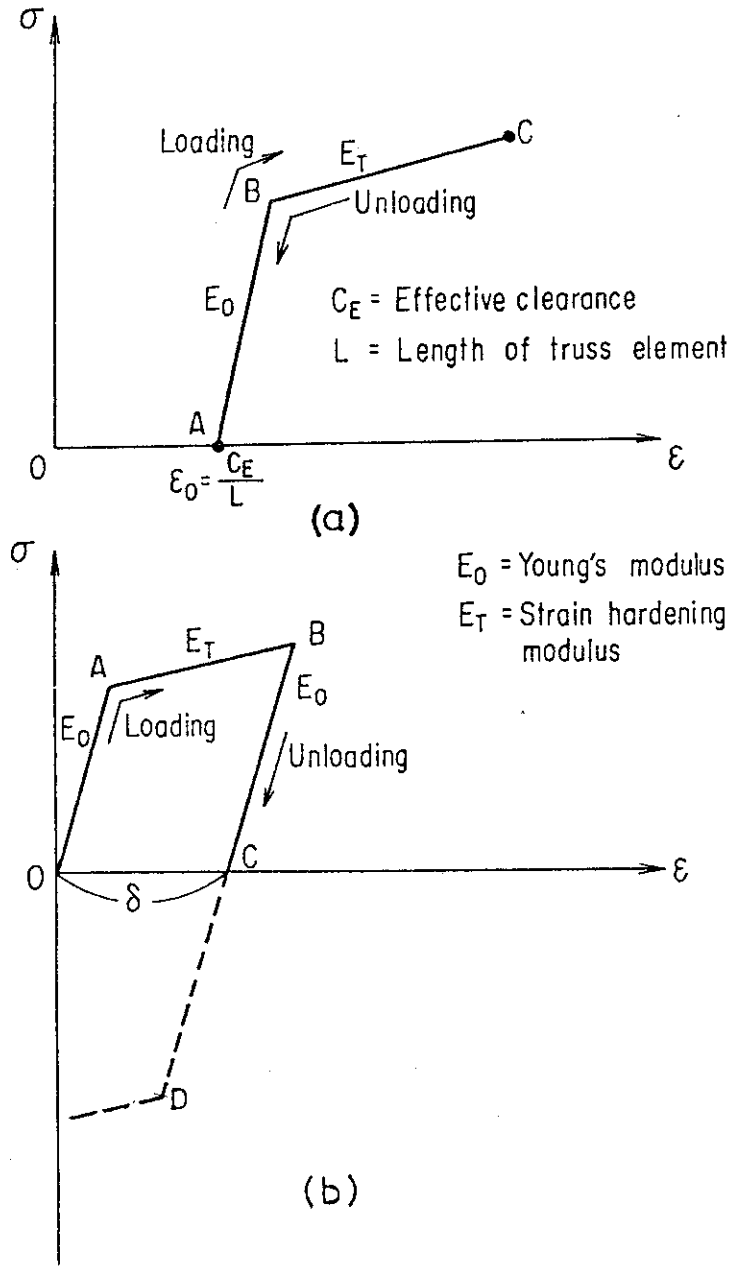

Fig. 18 Loading and unloading paths of the restraint